This paper appears in: IEEE Transactions on Systems, Man, and Cybernetics: Systems, 2022.
Digital Object Identifier: 10.1109/TSMC.2022.3144009

Dual-User Haptic Teleoperation of Complementary Motions of a Redundant Wheeled Mobile Manipulator Considering Task Priority

Hongjun Xing, Liang Ding, *Senior Member, IEEE*, Haibo Gao,
Weihua Li, and Mahdi Tavakoli, *Senior Member, IEEE*

***Abstract*—With the increasing applications of wheeled mobile manipulators (WMMs), consisting of a mobile platform (MP) and a manipulator, in diverse fields, new challenges have arisen in achieving multiple tasks such as obstacle avoidance in a constrained environment during the end-effector (EE) operation. A WMM is usually redundant due to the combination of the MP and the manipulator, making multi-task control possible via employing its null space. Dual-user/two-handed teleoperation of a WMM is desirable for tasks where it is important to simultaneously control the poses of both the MP and the EE. The existing teleoperation approaches for WMMs are mostly executed at the kinematic level, without considering the nonlinear rigid-body dynamics of the WMMs. In this paper, a task-priority-based dual-user teleoperation framework for a WMM is implemented to perform tasks in a constrained environment. It can simultaneously manipulate the MP and the EE, the overground obstacles are avoided by tele-controlling the MP using the WMM's null space. Any residual redundancy can be further employed for other tasks such as singularity avoidance. The stability of the entire teleoperation design is rigorously proved even with arbitrary time delays. Experiments with a dual-user teleoperation system, consisting of two local robots and an omnidirectional WMM, are conducted to verify the proposed approach's feasibility and effectiveness.**

***Index Terms*—Wheeled mobile manipulators, adaptive control, kinematic redundancy, task-priority based dual-user teleoperation, stability analysis.**

I. Introduction

Teleoperation has been widely employed in many applications, including search and rescue [1], [2], planetary exploration [3], and robotic surgical training [4], which extends an operator's sensing and operational capacity to a remote location. Wheeled mobile manipulators (WMMs) have found many applications, including human-robot cooperation, heavy object handling, and pick-and-place operation [5], [6] due to their satisfactory mobility and manipulation capability. However, in an unstructured environment such as rescue environment, the unexpected obstacles on the ground may impede the motion of the mobile platform (MP) during the task execution. In such a situation, a practical teleoperation approach for a WMM to simultaneously control the MP and the EE is required; refer to the supplementary material accompanying this manuscript for a motivating example. Besides, the WMM's complex dynamics also need to be handled.

Teleoperation of a WMM is vital in achieving remote task execution and providing a stable interaction with hazardous environments. In the following, we will use the terms "local" and "remote" instead of "master" and "slave". Notably, "remote robot" does not mean the robot is at a remote site but indicates that a local robot controls the robot. Park and Khatib [7] presented a teleoperation method for redundant WMMs using a virtual spring to connect the local and remote systems at the dynamic level. The redundancy resolution and telepresence were achieved by decomposing the task and posture dynamics, and on-line stiffness estimation. Nevertheless, a continuous inertia weighted pseudo-inverse was demanded to realize ideal decomposition. Garcia *et al.* [8] presented a teleoperation interface for WMMs considering the remote center of motion constraints, which could also include additional limitations via the system redundancy. However, a suitable planning method was required in the case of unstructured environments. In [9] and [10], a bilateral teleoperation approach for WMMs was proposed from kinematic and dynamic levels, respectively. The user could manually switch to control the MP or the EE using a single local robot. However, this strategy could not conduct some tasks requiring the MP and the EE simultaneously. Thus, multilateral teleoperation for WMMs is in demand.

The multilateral cooperative teleoperation framework was first proposed by Sirouspour [11], which achieved position/force tracking between the local and remote robots based on the μ-synthesis approach. From our group, Li *et al.* [12] proposed a dual-user teleoperation framework of using two local robots (1-DOF and 2-DOF) to control a 3-DOF single remote robot with system stability proved. Then, Agbalé *et al.* [13] evaluated the performance of using two 3-DOF haptic interfaces to operate a 6-DOF manipulator where the motions of the two local robots were complementary, which means the two local robots controlled the different DOFs of the

This work was supported by Canada Foundation for Innovation (CFI), the Natural Sciences and Engineering Research Council (NSERC) of Canada, the Canadian Institutes of Health Research (CIHR), the Alberta Advanced Education Ministry, the Alberta Economic Development, Trade and Tourism Ministry's grant to Centre for Autonomous Systems in Strengthening Future Communities, the National Natural Science Foundation of China (Grant No. 91948202, 51822502), the "111" Project (Grant No. B07018), and the China Scholarship Council under Grant [2019]06120165. (H. Xing and L. Ding contributed equally to this work. L. Ding and M. Tavakoli are the corresponding authors).

H. Xing, L. Ding, H. Gao, and W. Li are with the State Key Laboratory of Robotics and System, Harbin Institute of Technology, Harbin 150001, China. (e-mails: {xinghj, liangding, gaohaibo, liweihua}@hit.edu.cn).

W. Li is with the School of Automotive Engineering, Harbin Institute of Technology (Weihai), Weihai 264209, China.

H. Xing and M. Tavakoli are with the Department of Electrical and Computer Engineering, University of Alberta, Edmonton T6G 1H9, Alberta, Canada. (e-mail: mahdi.tavakoli@ualberta.ca).

manipulator. For example, one controlled the EE's position, and the other controlled its orientation. Malysz *et al.* [14], [15] proposed a trilateral two-local/one-remote teleoperation framework for kinematically redundant robots, where the first local robot operated the remote end-effector frame and the second local robot controlled a secondary objective, *e.g.*, realizing obstacle avoidance.

For a redundant WMM, its redundancy can be employed to control the MP's motion by assigning a secondary task. Farelo *et al.* [16] presented a dual-trajectory tracking control of a redundant WMM for a door-opening task, where the position and orientation of the MP were controlled by optimizing a cost function via its null space. However, the rotation and translation of the MP could not be achieved simultaneously during the task. To transparently execute the EE motion without interference from the motion of the MP, a task-priority framework can be utilized [17]. Mashali *et al.* [18] presented a task-priority-based dual-trajectory control for redundant WMM systems. The MP's pose was maintained within a range to the end-effector by adding two joint-dependent control variables. However, both these two dual-trajectory control approaches for WMMs were conducted at the kinematic level, without taking the complicated WMMs' dynamics into account.

In the literature, the investigation about teleoperation of WMMs shows that a general framework is to use only one single local robot. Multilateral teleoperation for priority-needed tasks is a useful technique with redundant robotic systems [15], [19]. However, no research has ever been conducted about employing two or more local robots to control a redundant WMM for multi-task execution. Task-priority-based redundancy resolution for redundant WMMs has been presented [18]. Nevertheless, it was conducted at the kinematic level, and a practical teleoperation framework remains unexplored.

This study aims to present a dual-user teleoperation approach to control a redundant WMM with two local robots. Besides tele-controlling the EE of the WMM (primary task) with the first local robot, the motion of the MP is tele-manipulated with the second local robot to realize obstacle avoidance (secondary task). When no singularity occurs, these two motions are independent; thus, we call them complementary motions to complete a complex task. The residual redundancy of the WMM system is further employed to avoid the manipulator's singular configuration (tertiary task). In summary, the main contributions of this work lie in: (1) A practical dual-user teleoperation framework for a redundant WMM with its EE and MP being separately controlled is proposed; (2) a joint-level Lyapunov-based adaptive controller is presented to handle the complicated nonlinear dynamics of the local robots and the remote robot/WMM, which can guarantee the stability of each system even in a contact environment; (3) a task-priority-based teleoperation framework for a redundant WMM is designed, which assigns each task with a priority level and guarantees that the high-priority task can be successfully executed without interference from any other tasks.

The remainder of this paper is organized as follows. Section II provides the dynamic models and joint-level adaptive controllers for the local and remote systems. In Section III, the required joint velocity commands for the local and remote systems are designed. Section IV describes the coordinated Cartesian-space velocity commands for the teleoperation system. Section V provides the stability proof of the approach. Experiments that demonstrate the proposed approach's validity and performance are presented in Section VI. Section VII concludes the manuscript.

II. Dynamics and Adaptive Control of Local/Remote Systems

In this section, the dynamic models for the local robots incorporating the human operators and the WMM integrating the environment have been established, respectively. An adaptive controller has also been proposed for each system to achieve a desirable joint position and velocity tracking.

A. Dynamics of Local Robots Incorporating Human Operators

As shown in [15], [20], the dynamics of a human operator can be assumed as a two-order linear-time-invariant (LTI) model

$$M_{ih}\ddot{x}_{ilo} + D_{ih}\dot{x}_{ilo} + K_{ih}x_{ilo} = f^*_{ih} - f_{ih}, \tag{1}$$

where $i = 1, 2$ denotes the first and the second local robots, respectively. $M_{ih} \in \mathbb{R}^{n_i \times n_i}$, $D_{ih} \in \mathbb{R}^{n_i \times n_i}$ and $K_{ih} \in \mathbb{R}^{n_i \times n_i}$ are all symmetric positive-definite matrices representing the inertia, damping and stiffness of the human arm, respectively, $x_{ilo} \in \mathbb{R}^{n_i}$ denotes the position vector of the point the human interacts with the local robot, and n_i is its Cartesian-space dimension. $f_{ih} \in \mathbb{R}^{n_i}$ is the force vector exerted by the operator to the corresponding local robot, $f^*_{ih} \in \mathbb{R}^{n_i}$ denotes the exogenous force vector generated by the operator subjected to

$$\|f^*_{ih}\|_\infty \leqslant \alpha_{ih} < +\infty, \tag{2}$$

where α_{ih} is a constant number.

The general form of the dynamic model for the local robots at joint space can be expressed as [21]

$$\begin{aligned} &M_{ilo}(q_{ilo})\ddot{q}_{ilo} + C_{ilo}(q_{ilo}, \dot{q}_{ilo})\dot{q}_{ilo} + \\ &G_{ilo}(q_{ilo}) + F_{f,ilo}(\dot{q}_{ilo}) = \tau_{ilo} + J^{\mathrm{T}}_{ilo}(q_{ilo})f_{ih}, \end{aligned} \tag{3}$$

where $q_{ilo} \in \mathbb{R}^{n_{ilo}}$ represents the joint configuration vector of the local robots, $M_{ilo} \in \mathbb{R}^{n_{ilo} \times n_{ilo}}$, $C_{ilo} \in \mathbb{R}^{n_{ilo} \times n_{ilo}}$, and $G_{ilo} \in \mathbb{R}^{n_{ilo}}$[1] denote the inertia matrix, the Coriolis and centrifugal matrices, and the gravitational torque vector of the corresponding local robot, respectively. $F_{f,ilo} \in \mathbb{R}^{n_{ilo}}$ is the joint friction torque vector, $\tau_{ilo} \in \mathbb{R}^{n_{ilo}}$ is the joint control torque vector, and $J_{ilo} \in \mathbb{R}^{n_i \times n_{ilo}}$ represents the Jacobian matrix of the local robots. Usually, the dynamic matrices in (3) possess the following two properties [22]

$$M_{ilo}(q_{ilo}) = M^{\mathrm{T}}_{ilo}(q_{ilo}) \geqslant \alpha I, \tag{4}$$

$$x^{\mathrm{T}}\big[\dot{M}_{ilo}(q_{ilo}) - 2C_{ilo}(q_{ilo}, \dot{q}_{ilo})\big]x = 0 \quad \forall x \in \mathbb{R}^{n_{ilo}}, \tag{5}$$

[1]Dependencies on q and $\dot{q}$ are usually shown at the first parameter introduction and omitted elsewhere for the sake of clarity.

where α represents a small positive scalar and I denotes an $n_{ilo} \times n_{ilo}$ identity matrix. According to (4), we can infer that M_{ilo}^{-1} exists and is positive-definite, and from (5), we can infer that $\dot{M}_{ilo} = C_{ilo} + C_{ilo}^{\mathrm{T}}$.

Combining (1) and (3), the dynamic model for the local robots incorporating the human operators can be expressed as

$$\mathscr{M}_{ilo}\ddot{q}_{ilo} + \mathscr{C}_{ilo}\dot{q}_{ilo} + \mathscr{G}_{ilo} + F_{f,ilo} = \tau_{ilo} + J_{ilo}^{\mathrm{T}} f_{ih}^{*} \tag{6}$$

with

$$\begin{aligned}
\mathscr{M}_{ilo} &= M_{ilo} + J_{ilo}^{\mathrm{T}} M_{ih} J_{ilo}, \\
\mathscr{C}_{ilo} &= C_{ilo} + J_{ilo}^{\mathrm{T}}(M_{ih}\dot{J}_{ilo} + D_{ih}J_{ilo}), \\
\mathscr{G}_{ilo} &= G_{ilo} + J_{ilo}^{\mathrm{T}} K_{ih} x_{ilo},
\end{aligned}$$

where $\dot{x}_{ilo} = J_{ilo}\dot{q}_{ilo}$ has been employed.

B. Dynamics of a Redundant WMM Incorporating Environment

The remote robot is a redundant WMM in this research, which may have contact with the environment. The dynamic behavior between the WMM's EE and the environment at the contact point can be illustrated using an impedance model, which is expressed as

$$M_e\ddot{x}_{ee} + D_e\dot{x}_{ee} + K_e(x_{ee} - x_{ee}^{\mathrm{o}}) = f_{ee}, \tag{7}$$

where $M_e \in \mathbb{R}^{n_1 \times n_1}$, $D_e \in \mathbb{R}^{n_1 \times n_1}$ and $K_e \in \mathbb{R}^{n_1 \times n_1}$ are symmetric positive-definite matrices representing the inertia, damping and stiffness of the contact, respectively, $x_{ee} \in \mathbb{R}^{n_1}$ denotes the EE's position vector, $x_{ee}^{\mathrm{o}} \in \mathbb{R}^{n_1}$ represents the position of the environment, and n_1 stands for the dimension of the Cartesian space the WMM interacts with the environment. $f_{ee} \in \mathbb{R}^{n_1}$ is the interaction force vector generated between the WMM and the environment, which can be measured by an F/T sensor or estimated based on an observer approach [23]. It is worth mentioning that the Cartesian-space dimensions of the EE and the first human operator are the same (denoted as n_1) since the first operator controls the EE.

According to [6], the forward kinematics mapping (at velocity level) for a WMM can be expressed as

$$\begin{aligned}
\dot{x}_{ee} &= J_u(q_{re})\dot{q}_{re} = \begin{bmatrix} J_{mp}(q_{re}) & J_{ma}(q_{re}) \end{bmatrix} \begin{bmatrix} \dot{q}_{mp} \\ \dot{q}_{ma} \end{bmatrix} \\
&= \begin{bmatrix} J_{mp}(q_{re}) & J_{ma}(q_{re}) \end{bmatrix} \begin{bmatrix} P(q_{mp})v_{mp} \\ v_{ma} \end{bmatrix} \\
&= J_{1re}(q_{re})v_{re},
\end{aligned} \tag{8}$$

where $q_{re} = [q_{mp}^{\mathrm{T}}, q_{ma}^{\mathrm{T}}]^{\mathrm{T}} \in \mathbb{R}^{n_{re}}$, $q_{mp} \in \mathbb{R}^{n_{mp}}$, and $q_{ma} \in \mathbb{R}^{n_{ma}}$ are the joint configuration vector of the remote robot (WMM), the MP, and the manipulator arm, respectively. $v_{re} = [v_{mp}^{\mathrm{T}}, v_{ma}^{\mathrm{T}}]^{\mathrm{T}} \in \mathbb{R}^{\bar{n}_{re}}$, $v_{mp} \in \mathbb{R}^{\bar{n}_{mp}}$, and $v_{ma} \in \mathbb{R}^{n_{ma}}$ are the velocity input vector of the WMM, the MP, and the manipulator arm, respectively. $P \in \mathbb{R}^{n_{mp} \times \bar{n}_{mp}}$ is the constraint matrix of the MP (holonomic or nonholonomic), which transfers the wheel velocities to the generalized mobile platform velocities. $J_{mp} \in \mathbb{R}^{n_1 \times n_{mp}}$ is the Jacobian of the MP related to the EE velocity vector, $J_{ma} \in \mathbb{R}^{n_1 \times n_{ma}}$ is the Jacobian of the manipulator related to the EE velocity vector, $J_u \in \mathbb{R}^{n_1 \times n_{re}}$ is the Jacobian of the unconstrained WMM, and $J_{1re} \in \mathbb{R}^{n_1 \times \bar{n}_{re}}$ is the Jacobian of the WMM.

To independently control the MP using another controller, the forward kinematics mapping of the MP can be computed as

$$\dot{x}_{mp} = J_p(q_{mp})v_{mp} = J_{2re}(q_{mp})v_{re}, \tag{9}$$

where $\dot{x}_{mp} \in \mathbb{R}^{n_2}$ denotes the MP's velocity vector with n_2 being its Cartesian-space dimension, $J_p \in \mathbb{R}^{n_2 \times \bar{n}_{mp}}$ represents the Jacobian of the MP related to its velocity vector, and $J_{2re} = [J_p, 0_{n_2 \times n_{ma}}] \in \mathbb{R}^{n_2 \times \bar{n}_{re}}$ is the extended Jacobian of the MP for the following controller design.

Define the extended joint configuration vector of the WMM as $q_{ere} = [q_{re}^{\mathrm{T}}, v_{mp}^{\mathrm{T}}]^{\mathrm{T}} \in \mathbb{R}^{n_{re}+\bar{n}_{mp}}$. Then according to [24], [25], the dynamic model of a WMM can be expressed as

$$\begin{aligned}
&M_{ere}(q_{ere})\ddot{q}_{ere} + C_{ere}(q_{ere}, \dot{q}_{ere})\dot{q}_{ere} + G_{ere}(q_{ere}) + \\
&F_{f,ere}(\dot{q}_{ere}) = E_{ere}\tau_{re} + A^{\mathrm{T}}(q_{ere})\lambda - J_{ere}^{\mathrm{T}} f_{ee}, \\
&A\dot{q}_{ere} = 0,
\end{aligned} \tag{10}$$

where $M_{ere} \in \mathbb{R}^{(n_{re}+\bar{n}_{mp}) \times (n_{re}+\bar{n}_{mp})}$, $C_{ere} \in \mathbb{R}^{(n_{re}+\bar{n}_{mp}) \times (n_{re}+\bar{n}_{mp})}$, and $G_{ere} \in \mathbb{R}^{n_{re}+\bar{n}_{mp}}$ denote the inertia matrix, the Coriolis and centrifugal matrices, and the gravitational torque vector of the WMM, respectively. $F_{f,ere} \in \mathbb{R}^{n_{re}+\bar{n}_{mp}}$ represents the joint friction torque vector and $\tau_{re} \in \mathbb{R}^{\bar{n}_{re}}$ is the actual joint torque input vector. $E_{ere} \in \mathbb{R}^{(n_{re}+\bar{n}_{mp}) \times \bar{n}_{re}}$ and $J_{ere} \in \mathbb{R}^{n_1 \times (n_{re}+\bar{n}_{mp})}$ map the joint torque input vector and the external force vector to the joint space, respectively. The matrix J_{ere} satisfies the condition that $\dot{x}_{ee} = J_{ere}\dot{q}_{ere}$. $A \in \mathbb{R}^{n_c \times (n_{re}+\bar{n}_{mp})}$ denotes kinematic constraint matrix, $\lambda \in \mathbb{R}^{n_c}$ represents the constraint force vector, and the superscript n_c is the number of the constraints. It should be noted that the matrices P and A are two different forms for expressing the kinematic constraints of the mobile platform [26].

With the transformation $\dot{q}_{ere} = S_{ere}v_{re}$, we can premultiply the first equation of (10) by S_{ere}^{T}. Then, along with the property $S_{ere}^{\mathrm{T}}A^{\mathrm{T}} = 0$, the unconstrained reduced form of the WMM dynamic model can be expressed as

$$M_{re}\dot{v}_{re} + C_{re}v_{re} + G_{re} + F_{f,re} = E_{re}\tau_{re} - J_{1re}^{\mathrm{T}} f_{ee}, \tag{11}$$

where $M_{re} = S_{ere}^{\mathrm{T}} M_{ere} S_{ere}$, $C_{re} = S_{ere}^{\mathrm{T}}(M_{ere}\dot{S}_{ere} + C_{ere}S_{ere})$, $G_{re} = S_{ere}^{\mathrm{T}} G_{ere}$, $F_{f,re} = S_{ere}^{\mathrm{T}} F_{f,ere}$, $E_{re} = S_{ere}^{\mathrm{T}} E_{ere}$, and $J_{1re}^{\mathrm{T}} = S_{ere}^{\mathrm{T}} J_{ere}^{\mathrm{T}}$. The last equation can be derived via $\dot{x}_{ee} = J_{ere}\dot{q}_{ere} = J_{1re}v_{re}$ and $\dot{q}_{ere} = S_{ere}v_{re}$. It is noteworthy that the above-mentioned model for WMMs is only applicable when no slippage or skidding between the wheels and the ground. For modelling of slippery wheels, one can refer our other publication [3].

Then, substituting the impedance model of the environment (7) into the reduced form of the WMM dynamic model (11), we can obtain the combined dynamic model for the WMM incorporating the environment as

$$\mathscr{M}_{re}\dot{v}_{re} + \mathscr{C}_{re}v_{re} + \mathscr{G}_{re} + F_{f,re} = E_{re}\tau_{re} \tag{12}$$

with

$$\begin{aligned}
\mathscr{M}_{re} &= M_{re} + J_{1re}^{\mathrm{T}} M_e J_{1re}, \\
\mathscr{C}_{re} &= C_{re} + J_{1re}^{\mathrm{T}}(M_e\dot{J}_{1re} + D_e J_{1re}), \\
\mathscr{G}_{re} &= G_{re} + J_{1re}^{\mathrm{T}} K_e(x_{ee} - x_{ee}^{\mathrm{o}}),
\end{aligned}$$

where $\dot{x}_{ee} = J_{1re} v_{re}$ has been employed. It is worth mentioning that the properties in (4) and (5) are also preserved in the combined dynamic models (6) and (12).

C. Joint-Level Adaptive Control Design

The goal of the joint-level adaptive control approach is to realize desirable joint position and velocity tracking without the requirement of the robotic system's exact dynamic parameters. Inspired by [20], and according to the combined dynamic model (6), the adaptive control law for the local systems[2] is designed as

$$\begin{aligned} \tau_{ilo} &= Y_{ilo}\hat{\theta}_{ilo} + \mathcal{K}_{ilo}\rho_{ilo} + \alpha_{ih} J_{ilo}^{\mathrm{T}} \mathrm{sign}(J_{ilo}\rho_{ilo}), \\ \rho_{ilo} &\overset{def}{=} \dot{q}_{ilo}^{r} - \dot{q}_{ilo} - J_{ilo}^{\dagger} \Upsilon_i \tilde{f}_{ih} \end{aligned} \tag{13}$$

subject to

$$\begin{aligned} Y_{ilo}\theta_{ilo} =& \mathscr{M}_{ilo} \frac{\mathrm{d}}{\mathrm{d}t}(\dot{q}_{ilo}^{r} - J_{ilo}^{\dagger}\Upsilon_i \tilde{f}_{ih}) + \\ & \mathscr{C}_{ilo}(\dot{q}_{ilo}^{r} - J_{ilo}^{\dagger}\Upsilon_i \tilde{f}_{ih}) + \mathscr{G}_{ilo} + F_{f,ilo}. \end{aligned} \tag{14}$$

According to (12), the adaptive control law for the remote system is designed as

$$\begin{aligned} E_{re}\tau_{re} &= Y_{re}\hat{\theta}_{re} + \mathcal{K}_{re}\rho_{re}, \\ \rho_{re} &\overset{def}{=} v_{re}^{r} - v_{re} - J_{1re}^{\dagger}\Upsilon_1 \tilde{f}_{ee} \end{aligned} \tag{15}$$

subject to

$$\begin{aligned} Y_{re}\theta_{re} =& \mathscr{M}_{re} \frac{\mathrm{d}}{\mathrm{d}t}(v_{re}^{r} - J_{1re}^{\dagger}\Upsilon_1 \tilde{f}_{ee}) + \\ & \mathscr{C}_{re}(v_{re}^{r} - J_{1re}^{\dagger}\Upsilon_1 \tilde{f}_{ee}) + \mathscr{G}_{re} + F_{f,re}. \end{aligned} \tag{16}$$

Here, we use γ to replace ilo or re to simplify the explanation. In the adaptive controllers (13)-(16), $\dot{q}_{ilo}^{r}$ and v_{re}^{r} represent the required joint velocity vector for the local robots and the WMM to be provided later, respectively. $\mathcal{K}_\gamma$ represents a positive diagonal gain matrix; $Y_\gamma\theta_\gamma$ represents the linearized dynamic model of the corresponding system, where Y_γ is the regressor matrix and θ_γ denotes the unknown parameter vector. $\Upsilon_1 \in \mathbb{R}^{n_1 \times n_1}$ and $\Upsilon_2 \in \mathbb{R}^{n_2 \times n_2}$ denote two diagonal positive-definite matrices with small elements. $J_\gamma^{\dagger} = W_\gamma^{-1} J_\gamma^{\mathrm{T}} (J_\gamma W_\gamma^{-1} J_\gamma^{\mathrm{T}})^{-1}$ denotes the weighted pseudoinverse of J_γ with W_γ being a symmetric and positive-definite weighting matrix [27], and this definition is applicable for all Jacobian pseudoinverse in this paper. $\tilde{f}_{ih}$ and $\tilde{f}_{ee}$ represent the filtered force vectors of f_{ih} and f_{ee} governed by

$$\dot{\tilde{Q}} + C\tilde{Q} = CQ, \tag{17}$$

where Q is the variable and C denotes a diagonal positive-definite matrix representing the filter bandwidth. It is noteworthy that the sign term in (13) is adopted to cope with the bounded exogenous force f_{ih}^{*}, and the implementation of the Υ term is to guarantee the asymptotic motion tracking for the local robots and the WMM even when contact occurs. In experimental implementation, f_{ih}^{*} is included in the forward compensation term $Y_{ilo}\theta_{ilo}$ to avoid the undesirable chattering, and this attempt presents acceptable results when the control rate is much higher than the change rate of f_{ih}^{*} [14], [20].

The value of $\hat{\theta}_\gamma$ can be updated using the $\mathcal{P}$ function provided in Definition 1 of the supplementary material with

$$s_\gamma = Y_\gamma^{\mathrm{T}} \rho_\gamma. \tag{18}$$

Then, each element of $\hat{\theta}_\gamma$ can be updated as

$$\hat{\theta}_{\gamma i} = \mathcal{P}(s_{\gamma i}, \varrho_{\gamma i}, \underline{\theta}_{\gamma i}, \overline{\theta}_{\gamma i}, t), \tag{19}$$

where $\hat{\theta}_{\gamma i}$ is the i^{th} element of $\hat{\theta}_\gamma$, $s_{\gamma i}$ is the i^{th} element of s_γ, $\varrho_{\gamma i} > 0$ is the update gain, and $\underline{\theta}_{\gamma i}$ and $\overline{\theta}_{\gamma i}$ are the lower bound and the upper bound of $\theta_{\gamma i}$.

Combining the dynamics of the local systems (6) with the adaptive control law (13)-(14), we can derive the local closed-loop dynamics as

$$\begin{aligned} -Y_{ilo}\tilde{\theta}_{ilo} = \mathscr{M}_{ilo}\dot{\rho}_{ilo} + \mathscr{C}_{ilo}\rho_{ilo} + \mathcal{K}_{ilo}\rho_{ilo} + \\ J_{ilo}^{\mathrm{T}}[f_{ih}^{*} + \alpha_{ih}\mathrm{sign}(J_{ilo}\rho_{ilo})], \end{aligned} \tag{20}$$

where $\tilde{\theta}_{ilo} = \hat{\theta}_{ilo} - \theta_{ilo}$ represents the estimate error vector for the unknown parameter.

Similarly, combining the dynamics of the remote system (12) with the adaptive control law (15)-(16), we can derive the remote closed-loop dynamics as

$$-Y_{re}\tilde{\theta}_{re} = \mathscr{M}_{re}\dot{\rho}_{re} + \mathscr{C}_{re}\rho_{re} + \mathcal{K}_{re}\rho_{re}, \tag{21}$$

where $\tilde{\theta}_{re} = \hat{\theta}_{re} - \theta_{re}$ represents the estimate error vector for the unknown parameter.

Define the candidate Lyapunov function as

$$V_\gamma = \frac{1}{2}\rho_\gamma^{\mathrm{T}}\mathscr{M}_\gamma\rho_\gamma + \frac{1}{2}\tilde{\theta}_\gamma^{\mathrm{T}}\varrho_\gamma^{-1}\tilde{\theta}_\gamma, \tag{22}$$

with the assumption that the actual values of the unknown parameters in θ_γ are constant, the following conclusion can be derived according to (2), (4), (5), (18)-(21) as

$$\dot{V}_\gamma \leqslant -\rho_\gamma^{\mathrm{T}}\mathcal{K}_\gamma\rho_\gamma. \tag{23}$$

Then, according to Lemma 1 in the supplementary material, (13), and (15), it derives

$$\begin{aligned} \rho_{1lo} &\overset{def}{=} \dot{q}_{1lo}^{r} - \dot{q}_{1lo} - J_{1lo}^{\dagger}\Upsilon_1\tilde{f}_{1h} \in L_2 \cap L_\infty, \\ \rho_{2lo} &\overset{def}{=} \dot{q}_{2lo}^{r} - \dot{q}_{2lo} - J_{2lo}^{\dagger}\Upsilon_2\tilde{f}_{2h} \in L_2 \cap L_\infty, \\ \rho_{re} &\overset{def}{=} v_{re}^{r} - v_{re} - J_{1re}^{\dagger}\Upsilon_1\tilde{f}_{ee} \in L_2 \cap L_\infty. \end{aligned} \tag{24}$$

The superiority of this approach compared with [15] is that the introduction of the Υ term can guarantee each system's stability even in a contact environment. Besides, the research in [15] was limited to a lightweight redundant manipulator, not a practical mobile manipulator, thus without considering the possible nonholonomic constraints of the mobile platform. The dynamic modeling of a complex mobile manipulator is also a light spot of this paper.

It is noteworthy that the application of these joint-level local adaptive controllers demands only the joint position/velocity feedback q_{ilo}/q_{re}, $\dot{q}_{ilo}/v_{re}$, the required joint velocity/acceleration command $\dot{q}_{ilo}^{r}/v_{re}^{r}$, $\ddot{q}_{ilo}^{r}/\dot{v}_{re}^{r}$, and the external force measurement f_{ih}/f_{ee}. The main advantage of the joint-level adaptive controllers is the avoidance of the joint acceleration measurement and the derivative of the external force.

[2]Hereinafter, we refer to the local robot incorporating the corresponding operator as the local system and the WMM incorporating the environment as the remote system.

III. Joint Velocity Command Design for Local and Remote Systems

This section provides the joint velocity commands for both the local and remote systems, where the task-priority-based redundancy resolution for the WMM is considered. Besides, a manipulability measure and a transition function are provided to avoid the manipulator's singularity and keep the continuity of the joint velocity command for the WMM, respectively.

A. Joint Velocity Command for Local Robots

The inverse kinematics mapping for the local robots can be expressed as $\dot{q}_{ilo} = J_{ilo}^{\dagger}\dot{x}_{ilo}$. Then, the required joint velocity command for them can be designed as $\dot{q}_{ilo}^{r} = J_{ilo}^{\dagger}\dot{x}_{ilo}^{r}$, where $\dot{x}_{ilo}^{r} \in \mathbb{R}^{n_i}$ denotes the required Cartesian-space velocity vector to be provided later. According to (13), (15), and (24), the following conclusion can be derived

$$\overline{\rho}_{ilo} \overset{def}{=} J_{ilo}\rho_{ilo} = \dot{x}_{ilo}^{r} - \dot{x}_{ilo} - \Upsilon_i \tilde{f}_{ih} \in L_2 \cap L_\infty \tag{25}$$

with the assumption that the Jacobian matrix J_{ilo} is bounded, which is invariably correct for manipulators with only prismatic or revolute joints.

B. Joint Velocity Command for a WMM

An approach to employing two controllers is to come up with one controller for the EE (primary task) and the other for the MP (secondary task). To avoid the interference between the two tasks, the prioritized task framework [28], [29] is adopted here.

According to (8), the joint velocity vector of the WMM with a given Cartesian-space velocity vector for the EE can be calculated as [17]

$$v_{re} = J_{1re}^{\dagger}\dot{x}_{ee} + N_{1re}\mu_1, \tag{26}$$

where $N_{1re} = I - J_{1re}^{\dagger}J_{1re}$ represents the orthogonal projector in the Jacobian null space, and μ_1 is an arbitrary joint velocity.

The pseudoinverse approach introduced above cannot avoid the joint position constraints when it is encountered. In this case, there are two other control methods available. One is Hierarchical Quadratic Programming (HQP) [30], which is usually implemented for robots to realize motion planning when multiple and incompatible constraints are involved. The other is to add joint limit avoidance as an optimization objective [31]. For controlling a WMM, the task-space position of its EE in the vertical direction is usually limited by the user. The EE's horizontal plane motion is mostly distributed to the MP with an unlimited joint motion range. Thus, the WMM will not encounter joint constraints using the presented null-space control approach.

According to (9) and (26), the Cartesian-space velocity vector of the MP for obstacle avoidance is expressed as

$$\dot{x}_{mp} = J_{2re}v_{re} = J_{2re}J_{1re}^{\dagger}\dot{x}_{ee} + J_{2re}N_{1re}\mu_1, \tag{27}$$

then, choose μ_1 to meet, if possible, also the secondary task as

$$\mu_1 = (J_{2re}N_{1re})^{\dagger}(\dot{x}_{mp} - J_{2re}J_{1re}^{\dagger}\dot{x}_{ee}) + N_{2|1re}\mu_2, \tag{28}$$

where $N_{2|1re} = I - (J_{2re}N_{1re})^{\dagger}(J_{2re}N_{1re})$ and μ_2 represents the available joint velocity vector for execution of a tertiary task. Finally, substituting (28) into (26) derives the general WMM kinematic model as

$$\begin{aligned} v_{re} = {} & J_{1re}^{\dagger}\dot{x}_{ee} + N_{1re}(J_{2re}N_{1re})^{\dagger} \\ & (\dot{x}_{mp} - J_{2re}J_{1re}^{\dagger}\dot{x}_{ee}) + N_{1re}N_{2|1re}\mu_2, \end{aligned} \tag{29}$$

thus, according to (29), the required joint velocity vector v_{re}^{r} for the WMM can be designed as

$$\begin{aligned} v_{re}^{r} = {} & J_{1re}^{\dagger}\dot{x}_{ee}^{r} + N_{1re}(J_{2re}N_{1re})^{\dagger} \\ & (\dot{x}_{mp}^{r} - J_{2re}J_{1re}^{\dagger}\dot{x}_{ee}^{r}) + N_{1re}N_{2|1re}\mu_2^{r}, \end{aligned} \tag{30}$$

where $\dot{x}_{ee}^{r}$, $\dot{x}_{mp}^{r}$, and μ_2^{r} represent the required Cartesian-space command vectors for $\dot{x}_{ee}$, $\dot{x}_{mp}$, and μ_2, respectively.

Substituting (29) and (30) into the third equation of (24) derives

$$\begin{aligned} \rho_{re} = {} & N_{1re}(J_{2re}N_{1re})^{\dagger}[\dot{x}_{mp}^{r} - \dot{x}_{mp} - J_{2re}J_{1re}^{\dagger} \\ & (\dot{x}_{ee}^{r} - \dot{x}_{ee})] - J_{1re}^{\dagger}\Upsilon_1\tilde{f}_{ee} + J_{1re}^{\dagger}(\dot{x}_{ee}^{r} - \dot{x}_{ee}) + \\ & N_{1re}N_{2|1re}(\mu_2^{r} - \mu_2) \in L_2 \cap L_\infty. \end{aligned} \tag{31}$$

Premultiplying (31) by J_{1re}, J_{2re}, and $N_{1re}N_{2|1re}$, respectively, and according to (8)-(11) in the supplementary material, one can obtain

$$\overline{\rho}_{1re} \overset{def}{=} J_{1re}\rho_{re} = \dot{x}_{ee}^{r} - \dot{x}_{ee} - \Upsilon_1\tilde{f}_{ee} \in L_2 \cap L_\infty, \tag{32}$$

$$\overline{\rho}_{2re} \overset{def}{=} J_{2re}\rho_{re} = \dot{x}_{mp}^{r} - \dot{x}_{mp} - J_{2re}J_{1re}^{\dagger}\Upsilon_1\tilde{f}_{ee} \in L_2 \cap L_\infty, \tag{33}$$

$$\overline{\rho}_{Nre} \overset{def}{=} N_{1re}N_{2|1re}\rho_{re} = N_{1re}N_{2|1re}(\mu_2^{r} - \mu_2) \in L_2 \cap L_\infty. \tag{34}$$

C. Singularity Avoidance Approach

Considering that the manipulator might be brought into a singular configuration due to the conflict of the two tasks (EE motion and MP motion), one can utilize the remaining DOFs of the WMM to keep the manipulator away from singularity. Further, an efficient approach to maintain joint velocity continuity is still required when singularity inextricably occurs. Here, we employ the velocity manipulability ellipsoid, an effective measure to evaluate the distance of a robot from its singularity [32], to optimize the WMM's configuration. For the manipulator, it is defined as $w(q_{ma}) = \sqrt{\det\left(J_{ma}J_{ma}^{\mathrm{T}}\right)}$. Instead of employing $w(q_{ma})$ as the optimization objective, we choose the cost function as $H(q_{ma}) = w^2(q_{ma})$ to make the configuration optimization more computationally efficient. The computation of the partial derivative of H over q_{ma} avoids the square root of $\det\left(J_{ma}J_{ma}^{\mathrm{T}}\right)$. Here, the tertiary task is defined as manipulability enhancement, and the required joint velocity vector for this task is designed as

$$\mu_2^{r} = \eta \begin{bmatrix} 0_{\bar{n}_{mp}\times 1} \\ (\nabla_{q_{ma}}H)^{\mathrm{T}} \end{bmatrix}, \tag{35}$$

where η is a positive control gain, and each element in $\nabla_{q_{ma}}H$ can be computed as $\nabla_{q_{ma,i}}H = 2\det(J_{ma}J_{ma}^{\mathrm{T}})\mathrm{tr}[\frac{\partial J_{ma}}{\partial q_{ma,i}}J_{ma}^{\dagger}]$, $i = 1, 2, \cdots, n_{ma}$. When the manipulator is too close to a

singularity, resulting in the rank deficiency of $J_{2re}N_{1re}$, then, the following damped least-squares pseudoinverse

$$J^{\dagger} = W^{-1}J^{\mathrm{T}}(JW^{-1}J^{\mathrm{T}} + k_d I)^{-1} \tag{36}$$

can be applied for $J_{2re}N_{1re}$ with

$$k_d = \begin{cases} -k_0 \sin(\frac{\pi}{2}\frac{\sigma_{ma}}{\sigma_{ma,\min}}) + k_0, & \text{if} \quad \sigma_{ma} < \sigma_{ma,\min} \\ 0, & \text{if} \quad \sigma_{ma} \geqslant \sigma_{ma,\min} \end{cases} \tag{37}$$

where k_0 is a positive number to keep system stability at the singularity, σ_{ma} is the minimum singular value of J_{ma}, and the singularity measure is denoted as $\sigma_{ma,\min}$.

IV. Required Cartesian-Space Velocity Command for Teleoperation

Section IV-A presents the required velocity design of the primary task teleoperation subsystem (the first local robot and the WMM's EE). Section IV-B shows the required velocity design of the secondary task teleoperation subsystem (the second local robot and the WMM's MP).

A. Required Velocity Vector of Primary Task Teleoperation Subsystem

The required velocity vectors for the first local robot and the EE in the Cartesian space are designed as

$$\begin{aligned} \dot{x}^{r}_{1lo} = k_{p1}^{-1}\Big\{ & \dot{\tilde{x}}_{ee} + \Lambda_1(\tilde{x}_{ee} - k_{p1}x_{1lo}) - \\ & \Upsilon_1\big[\tilde{f}_{ee} - (k_{f1}+k_{p1})\tilde{f}_{1h}\big]\Big\} - \epsilon_1\dot{\tilde{x}}_{1lo}, \end{aligned} \tag{38}$$

$$\dot{x}^{r}_{ee} = k_{p1}\dot{\tilde{x}}_{1lo} + \Lambda_1(k_{p1}\tilde{x}_{1lo} - x_{ee}) + \Upsilon_1 k_{f1}\tilde{f}_{1h} - \epsilon_1\dot{\tilde{x}}_{ee}, \tag{39}$$

where $k_{p1} \in \mathbb{R}^{n_1\times n_1}$ and $k_{f1} \in \mathbb{R}^{n_1\times n_1}$ represent diagonal positive-definite position scaling and force scaling matrices, respectively, $\Lambda_1 \in \mathbb{R}^{n_1\times n_1}$ and $\epsilon_1 \in \mathbb{R}^{n_1\times n_1}$ denote two diagonal positive-definite matrices. The ϵ_1 term is added to improve this subsystem's transient response performance.

Substituting (38) and (39) into (25) and (32) derives

$$\overline{\rho}_{1re} - k_{p1}\overline{\rho}_{1lo} = [(I+\epsilon_1)s + \Lambda_1]\tilde{\mathcal{X}}_1 + (\Lambda_1 + s)\mathcal{X}_1, \tag{40}$$

$$\begin{aligned} \overline{\rho}_{1re} + k_{p1}\overline{\rho}_{1lo} = {} & k_{p1}(s+\Lambda_1)(\tilde{x}_{1lo} - x_{1lo}) - \epsilon_1 s(k_{p1}\tilde{x}_{1lo} + \\ & \tilde{x}_{ee}) + (s+\Lambda_1)(\tilde{x}_{ee} - x_{ee}) + 2\Upsilon_1(k_{f1}\tilde{f}_{1h} - \tilde{f}_{ee}), \end{aligned} \tag{41}$$

where $\mathcal{X}_1 \overset{def}{=} k_{p1}x_{1lo} - x_{ee}$ and s denotes the Laplace operator. According to (17), (40) can be rewritten as

$$\overline{\rho}_{1re} - k_{p1}\overline{\rho}_{1lo} = [C^{-1}s^2 + (C^{-1}\Lambda_1 + \epsilon_1 + 2I)s + 2\Lambda_1]\tilde{\mathcal{X}}_1. \tag{42}$$

By selecting $\epsilon_1 > -2I - C^{-1}\Lambda_1$ and utilizing Lemma 3 in the supplementary material, we can conclude that

$$\tilde{\mathcal{X}}_1 \in L_2 \cap L_\infty, \quad \dot{\tilde{\mathcal{X}}}_1 \in L_2 \cap L_\infty, \quad \ddot{\tilde{\mathcal{X}}}_1 \in L_2 \cap L_\infty. \tag{43}$$

Using (17) and (43), we can further conclude $\mathcal{X}_1 \in L_2 \cap L_\infty$ and $\dot{\mathcal{X}}_1 \in L_2 \cap L_\infty$. According to (56) in Section V, we can derive $\ddot{\mathcal{X}}_1 \in L_\infty$. Then employing Lemma 4 of the supplementary material, it derives

$$\lim_{t\to\infty} k_{p1}x_{1lo} - x_{ee} = 0, \quad \lim_{t\to\infty} k_{p1}\dot{x}_{1lo} - \dot{x}_{ee} = 0. \tag{44}$$

To obtain a desirable transient response, we select ϵ_1 as

$$\epsilon_1 = 2\sqrt{2}\Lambda_1^{\frac{1}{2}}C^{-\frac{1}{2}} - \Lambda_1 C^{-1} - 2I \tag{45}$$

to make (42) as a critically damped system. In view of (17), (41) is revised as

$$-\frac{\rho_{p1}}{2} = k_{p1}\Upsilon_1^{-1}(C^{-1}s + C^{-1}\Lambda_1 + \epsilon_1)\dot{\tilde{x}}_{1lo} - (k_{f1}\tilde{f}_{1h} - \tilde{f}_{ee}) \tag{46}$$

with

$$\rho_{p1} \overset{def}{=} \Upsilon_1^{-1}[(\overline{\rho}_{1re} + k_{p1}\overline{\rho}_{1lo}) - (C^{-1}s + C^{-1}\Lambda_1 + \epsilon_1)\dot{\tilde{\mathcal{X}}}_1].$$

According to (25), (32), and (43), it derives that $\rho_{p1} \in L_2 \cap L_\infty$. For the transparency of the primary task teleoperation subsystem, we can reword (46) as

$$\begin{aligned} \tilde{f}_{1h} = {} & k_{f1}^{-1}\tilde{f}_{ee} + \frac{k_{f1}^{-1}}{2}\rho_{p1} + \\ & k_{f1}^{-1}k_{p1}\Upsilon_1^{-1}(C^{-1}s + C^{-1}\Lambda_1 + \epsilon_1)\dot{\tilde{x}}_{1lo}, \end{aligned} \tag{47}$$

where the third term in the right-hand side makes the teleoperation system act as a free-floating mass $k_{f1}^{-1}k_{p1}\Upsilon_1^{-1}C^{-1}$ plus a damper $k_{f1}^{-1}k_{p1}\Upsilon_1^{-1}(C^{-1}\Lambda_1 + \epsilon_1)$. According to (56) in Section V, we can derive that $\dot{\rho}_{p1} \in L_\infty$. In view of Lemma 4 in the supplementary material, it can be concluded that $\lim_{t\to\infty}\rho_{p1} = 0$. Then, within the filter bandwidth C, we can conclude that the first user force and the scaled environment force can track each other. It is noteworthy that large Υ_1 and C can decrease the transparency error; however, this will bring instability to the control system [20]. Thus, the selection of Υ_1 and C is a trade-off between transparency and stability.

B. Required Velocity Vector of Secondary Task Teleoperation Subsystem

The required velocity commands for the second local robot and the MP in the Cartesian space are depicted as

$$\begin{aligned} \dot{x}^{r}_{2lo} = {} & k_{p2}^{-1}\big[\dot{\tilde{x}}_{mp} + \Lambda_2(\tilde{x}_{mp} - k_{p2}x_{2lo}) + \\ & \Upsilon_2(k_{f2}+k_{p2})\tilde{f}_{2h}\big] - \epsilon_2\dot{\tilde{x}}_{2lo}, \end{aligned} \tag{48}$$

$$\begin{aligned} \dot{x}^{r}_{mp} = {} & k_{p2}\dot{\tilde{x}}_{2lo} + \Lambda_2(k_{p2}\tilde{x}_{2lo} - x_{mp}) + \\ & \Upsilon_2 k_{f2}\tilde{f}_{2h} + J_{2re}J^{\dagger}_{1re}\Upsilon_1\tilde{f}_{ee} - \epsilon_2\dot{\tilde{x}}_{mp}, \end{aligned} \tag{49}$$

where $k_{p2} \in \mathbb{R}^{n_2\times n_2}$ and $k_{f2} \in \mathbb{R}^{n_2\times n_2}$ denote diagonal positive-definite position scaling and force scaling matrices, respectively, $\Lambda_2 \in \mathbb{R}^{n_2\times n_2}$ and $\epsilon_2 \in \mathbb{R}^{n_2\times n_2}$ represent two diagonal positive-definite matrices.

Substituting (48) and (49) into (25) and (33) derives

$$\overline{\rho}_{2re} - k_{p2}\overline{\rho}_{2lo} = [(I+\epsilon_2)s + \Lambda_2]\tilde{\mathcal{X}}_2 + (\Lambda_2 + s)\mathcal{X}_2, \tag{50}$$

$$\begin{aligned} \overline{\rho}_{2re} + k_{p2}\overline{\rho}_{2lo} = {} & k_{p2}(s+\Lambda_2)(\tilde{x}_{2lo} - x_{2lo}) - \epsilon_2 s(k_{p2} \\ & \tilde{x}_{2lo} + \tilde{x}_{mp}) + (s+\Lambda_2)(\tilde{x}_{mp} - x_{mp}) + 2\Upsilon_2 k_{f2}\tilde{f}_{2h}, \end{aligned} \tag{51}$$

where $\mathcal{X}_2 \overset{def}{=} k_{p2}x_{2lo} - x_{mp}$. Using the same approach demonstrated in Section IV-A. Selecting $\epsilon_2 > -2I - C^{-1}\Lambda_2$, we can conclude that

$$\begin{aligned} & \tilde{\mathcal{X}}_2 \in L_2 \cap L_\infty, \quad \dot{\tilde{\mathcal{X}}}_2 \in L_2 \cap L_\infty, \quad \ddot{\tilde{\mathcal{X}}}_2 \in L_2 \cap L_\infty, \\ & \mathcal{X}_2 \in L_2 \cap L_\infty, \quad \dot{\mathcal{X}}_2 \in L_2 \cap L_\infty, \\ & \lim_{t\to\infty} k_{p2}x_{2lo} - x_{mp} = 0, \quad \lim_{t\to\infty} k_{p2}\dot{x}_{2lo} - \dot{x}_{mp} = 0. \end{aligned} \tag{52}$$

Here, we choose $\epsilon_2 = 2\sqrt{2}\Lambda_2^{\frac{1}{2}}C^{-\frac{1}{2}} - \Lambda_2 C^{-1} - 2I$ to enhance the transient response of this teleoperation subsystem.

Rewriting (51) as

$$\tilde{f}_{2h} = \frac{k_{f2}^{-1}}{2}\rho_{p2} + k_{f2}^{-1}k_{p2}\Upsilon_2^{-1}(C^{-1}s + C^{-1}\Lambda_2 + \epsilon_2)\dot{\tilde{x}}_{2lo} \quad (53)$$

with

$$\rho_{p2} \overset{def}{=} \Upsilon_2^{-1}[(\overline{\rho}_{2re} + k_{p2}\overline{\rho}_{2lo}) - (C^{-1}s + C^{-1}\Lambda_2 + \epsilon_2)\dot{\tilde{\mathcal{X}}}_2].$$

In accordance with (25), (33), and (52), it derives that $\rho_{p2} \in L_2 \cap L_\infty$. As in Section IV-A, we can prove $\lim_{t\to\infty}\rho_{p2} = 0$ with $\dot{\rho}_{p2} \in L_\infty$ using (59) in Section V. From (53), the second operator feels a mass-damper impedance system, and in a quasi-static condition, it satisfies that $f_{2h} \approx 0$.

The block diagram of the proposed dual-user teleoperation system for a WMM is shown in Fig. 1, where Ξ represents the first-order filter expressed in (17). In Fig. 1, the control law of the first local robot is presented in the top left, the second local robot in the bottom left, and the remote robot (WMM) in the right column. The three control laws work independently for their respective systems, while their required task-space velocity commands are mutually connected. The data transmission between these systems is shown by a "Communication Channels" block for teleoperation.

V. Stability Analysis

A. Stability Without Time Delay

The overall stability proof for the primary/secondary task teleoperation and the tertiary task control subsystem is provided here. To simplify the analysis, $x_{ee}^o = 0$ in (7) is assumed. For the primary task teleoperation subsystem, according to (1), (7), (17), and (47), we can attain the following dynamic model

$$\begin{aligned}&\tilde{f}_{1h}^* + \overline{\rho}_{1e} = \big[M_{1h} + k_{f1}^{-1}k_{p1}(M_e + \Upsilon_1^{-1}C^{-1})\big]\ddot{\tilde{x}}_{1lo} + \\ &\big[D_{1h} + k_{f1}^{-1}k_{p1}(D_e + \Upsilon_1^{-1}C^{-1}\Lambda_1 + \Upsilon_1^{-1}\epsilon_1)\big]\dot{\tilde{x}}_{1lo} + \\ &(K_{1h} + k_{f1}^{-1}k_{p1}K_e)\tilde{x}_{1lo}\end{aligned} \quad (54)$$

with

$$\overline{\rho}_{1e} \overset{def}{=} k_{f1}^{-1}M_e\ddot{\tilde{\mathcal{X}}}_1 + k_{f1}^{-1}D_e\dot{\tilde{\mathcal{X}}}_1 + k_{f1}^{-1}K_e\tilde{\mathcal{X}}_1 - \frac{k_{f1}^{-1}}{2}\rho_{p1},$$

according to (43), it derives $\overline{\rho}_{1e} \in L_2 \cap L_\infty$. Then, using Lemmas 2 and 3 in the supplementary material, (2), and (17), we can obtain

$$x_{1lo}, x_{ee}, \dot{x}_{1lo}, \dot{x}_{ee}, \ddot{\tilde{x}}_{1lo}, \ddot{\tilde{x}}_{ee}, \dot{\tilde{x}}_{1lo}, \dot{\tilde{x}}_{ee}, \tilde{x}_{1lo}, \tilde{x}_{ee} \in L_\infty, \quad (55)$$

and combining (13), (15), (20), and (21), we can further derive

$$\ddot{x}_{1lo}^r, \ddot{x}_{1lo}, \ddot{x}_{ee}^r, \ddot{x}_{ee}, \dot{\tilde{f}}_{1lo}, \dot{\tilde{f}}_{ee} \in L_\infty. \quad (56)$$

Utilizing the same approach for the MP teleoperation subsystem, in view of (1), (2), (17), (52), and (53), it derives

$$\begin{aligned}&\tilde{f}_{2h}^* - \frac{k_{f2}^{-1}}{2}\rho_{p2} = (M_{2h} + k_{f2}^{-1}k_{p2}\Upsilon_2^{-1}C^{-1})\ddot{\tilde{x}}_{2lo} + \\ &(D_{2h} + k_{f2}^{-1}k_{p2}\Upsilon_2^{-1}C^{-1}\Lambda_2 + \Upsilon_2^{-1}\epsilon_2)\dot{\tilde{x}}_{2lo} + K_{2h}\tilde{x}_{2lo},\end{aligned} \quad (57)$$

thus,

$$x_{2lo}, x_{mp}, \dot{x}_{2lo}, \dot{x}_{mp}, \ddot{\tilde{x}}_{2lo}, \ddot{\tilde{x}}_{mp}, \dot{\tilde{x}}_{2lo}, \dot{\tilde{x}}_{mp}, \tilde{x}_{2lo}, \tilde{x}_{mp} \in L_\infty, \quad (58)$$

and further,

$$\ddot{x}_{2lo}^r, \ddot{x}_{2lo}, \ddot{x}_{mp}^r, \ddot{x}_{mp}, \dot{\tilde{f}}_{2lo} \in L_\infty. \quad (59)$$

The remaining redundancy of the WMM is used to execute the tertiary task. According to (34), the required joint velocity vector μ_2^r should be designed to meet $\mu_2^r \in L_\infty$ to ensure its motion in the corresponding null space is stable and bounded. This will be guaranteed if the required velocity vector is devised based on the gradient of some convex functions of joint configuration [33], such as (35). Thus, $\mu_2 \in L_\infty$.

B. Stability Under Time Delay

Time delay is an essential issue in teleoperation, especially for space application. Although this research focuses on terrestrial teleoperation, the robotic system's stability against arbitrary delays in the communication channels should be guaranteed. With time delay considered between the local robots and the WMM, for the primary task teleoperation subsystem, (38) and (39) should be revised as

$$\begin{aligned}\dot{x}_{1lo}^r = k_{p1}^{-1}\Big\{&e^{-sT_2}(\dot{\tilde{x}}_{ee} + \Lambda_1\tilde{x}_{ee}) - \Lambda_1 k_{p1}x_{1lo} - \\ &\Upsilon_1\big[e^{-sT_2}\tilde{f}_{ee} - (k_{f1} + k_{p1})\tilde{f}_{1h}\big]\Big\} - \epsilon_1\dot{\tilde{x}}_{1lo},\end{aligned} \quad (60)$$

$$\begin{aligned}\dot{x}_{ee}^r = &e^{-sT_1}k_{p1}(\dot{\tilde{x}}_{1lo} + \Lambda_1\tilde{x}_{1lo}) - \Lambda_1 x_{ee} + \\ &e^{-sT_1}k_{f1}\Upsilon_1\tilde{f}_{1h} - \epsilon_1\dot{\tilde{x}}_{ee},\end{aligned} \quad (61)$$

where T_1 and T_2 denote the time delays from the local side to the remote side and vice versa. Substituting (60) and (61) into (25) and (32) derives

$$\begin{aligned}&k_{p1}(\dot{x}_{1lo} + \Lambda_1 x_{1lo}) - k_{f1}\Upsilon_1\tilde{f}_{1h} + k_{p1}\epsilon_1\dot{\tilde{x}}_{1lo} = \\ &e^{-sT_2}(\dot{\tilde{x}}_{ee} + \Lambda_1\tilde{x}_{ee} - \Upsilon_1\tilde{f}_{ee}) - k_{p1}\overline{\rho}_{1lo},\end{aligned} \quad (62)$$

$$\begin{aligned}&\dot{x}_{ee} + \Lambda_1 x_{ee} + \Upsilon_1\tilde{f}_{ee} + \epsilon_1\dot{\tilde{x}}_{ee} = \\ &e^{-sT_1}\big[k_{p1}(\dot{\tilde{x}}_{1lo} + \Lambda_1\tilde{x}_{1lo}) + k_{f1}\Upsilon_1\tilde{f}_{1h}\big] - \overline{\rho}_{1re}.\end{aligned} \quad (63)$$

According to (1) and (7), we can represent the human dynamics and the environment dynamics as

$$\begin{aligned}f_{1h} &= -\mathcal{Z}_{1h}\dot{x}_{1lo} + f_{1h}^*, \\ f_{ee} &= \mathcal{Z}_e\dot{x}_{ee},\end{aligned} \quad (64)$$

where $\mathcal{Z}_{1h}$ and $\mathcal{Z}_e$ denote the mechanical impedance of the first operator and the environment, respectively. Then, it follows from (62) and (63) that

$$\mathcal{G}_{1lo1}(s)(k_{p1}\tilde{x}_{1lo}) = \mathcal{G}_{1lo2}(s)e^{-sT_2}(\tilde{x}_{ee}) - k_{p1}\underline{\rho}_{1lo}, \quad (65)$$

$$\mathcal{G}_{1re1}(s)(\tilde{x}_{ee}) = \mathcal{G}_{1re2}(s)e^{-sT_1}(k_{p1}\tilde{x}_{1lo}) - k_{p1}\underline{\rho}_{1re}. \quad (66)$$

The expression of some symbols in equations of this section can be found in the supplementary material.

In combination with (65) and (66), we can obtain

$$\begin{aligned}k_{p1}\tilde{x}_{1lo} = &\mathcal{G}_{1lo1}^{-1}(s)\mathcal{G}_{1lo2}(s)\mathcal{G}_{1re1}^{-1}(s)\mathcal{G}_{1re2}(s) \\ &e^{-s(T_1+T_2)}(k_{p1}\tilde{x}_{1lo}) - \rho_{1lo}^*,\end{aligned} \quad (67)$$

$$\begin{aligned}\tilde{x}_{ee} = &\mathcal{G}_{1re1}^{-1}(s)\mathcal{G}_{1re2}(s)\mathcal{G}_{1lo1}^{-1}(s)\mathcal{G}_{1lo2}(s) \\ &e^{-s(T_1+T_2)}(\tilde{x}_{ee}) - \rho_{1re}^*,\end{aligned} \quad (68)$$

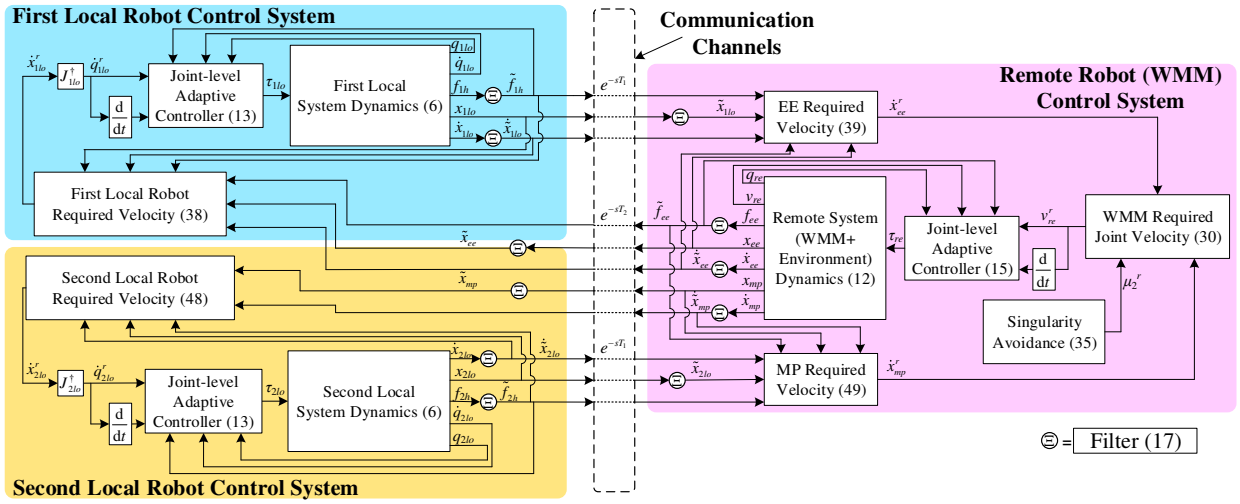

Fig. 1: Block diagram of the proposed teleoperation system.

Thus, the sufficient condition for stability under any time delay can be derived as

$$\begin{aligned}\left\|\mathcal{G}_{1lo1}^{-1}(j\omega)\mathcal{G}_{1lo2}(j\omega)\mathcal{G}_{1re1}^{-1}(j\omega)\mathcal{G}_{1re2}(j\omega)\right\|_\infty &< 1,\\ \left\|\mathcal{G}_{1re1}^{-1}(j\omega)\mathcal{G}_{1re2}(j\omega)\mathcal{G}_{1lo1}^{-1}(j\omega)\mathcal{G}_{1lo2}(j\omega)\right\|_\infty &< 1.\end{aligned} \tag{69}$$

According to [34], a sufficient condition for (69) is

$$\left\|\mathcal{G}_{1lo2}(j\omega)\mathcal{G}_{1re1}^{-1}(j\omega)\right\|_\infty < 1, \tag{70}$$

$$\left\|\mathcal{G}_{1lo1}^{-1}(j\omega)\mathcal{G}_{1re2}(j\omega)\right\|_\infty < 1. \tag{71}$$

Without loss of generality, we take a one-dimensional case as an example. The extension to multiple-dimensional cases can be analyzed accordingly. Similar to (1) and (7), we consider the first operator dynamics and the environment dynamics as (only one dimension is considered)

$$\begin{aligned}\mathcal{Z}_{1h} &= m_{1h}s + d_{1h} + k_{1h}/s,\\ \mathcal{Z}_e &= m_e s + d_e + k_e/s.\end{aligned} \tag{72}$$

Then, combining (65), (66), (70), (71), and (72), it derives

$$\left\|\mathscr{A}/\mathscr{B}\right\|_\infty < 1 \tag{73}$$

with $\mathscr{A} = -C\Upsilon_1\breve{m}(j\omega)^2 + (C - C\Upsilon_1\breve{d})(j\omega) + (C\Lambda_1 - C\Upsilon_1\breve{k})$ and $\mathscr{B} = (1 + C\Upsilon_1\breve{m})(j\omega)^2 + (C + \Lambda_1 + C\Upsilon_1\breve{d} + C\epsilon_1)(j\omega) + (C\Lambda_1 + C\Upsilon_1\breve{k})$, where for (70), $\breve{m} = m_e$, $\breve{d} = d_e$, $\breve{k} = k_e$, and for (71), $\breve{m} = (k_{f1}/k_{p1})m_{1h}$, $\breve{d} = (k_{f1}/k_{p1})d_{1h}$, $\breve{k} = (k_{f1}/k_{p1})k_{1h}$.

To meet the requirement of (73), the following condition should be satisfied

$$\begin{aligned}&\left[(C\Lambda_1 + C\Upsilon_1\breve{k}) - (1 + C\Upsilon_1\breve{m})\omega^2\right]^2 +\\ &\left[(C + \Lambda_1 + C\Upsilon_1\breve{d} + C\epsilon_1)\omega\right]^2 - \left[(C - C\Upsilon_1\breve{d})\omega\right]^2 -\\ &\left[(C\Lambda_1 - C\Upsilon_1\breve{k}) + C\Upsilon_1\breve{m}\omega^2\right]^2 > 0\end{aligned} \tag{74}$$

for both the first local robot and the end-effector. Simplifying (74) derives

$$a_1\omega^4 + b_1\omega^2 + c_1 > 0. \tag{75}$$

Due to the positive-definite properties of $\breve{m}$, $\breve{d}$, $\breve{k}$, Λ_1, and Υ_1, it derives $a_1 > 0$ and $c_1 > 0$ unconditionally. Then, the following condition must hold to guarantee (75),

$$b_1 + 4C\sqrt{\Lambda_1\Upsilon_1\breve{k}(1 + 2C\Upsilon_1\breve{m})} > 0. \tag{76}$$

Thus, by appropriately selecting control parameters to satisfy (75) and (76), the stability of the primary task teleoperation subsystem under any time delay can be guaranteed.

The stability proof of the secondary task teleoperation subsystem under time delay can be derived using a similar approach to the primary subsystem. Assume that the second operator's dynamics are $f_{2h} = -\mathcal{Z}_{2h}\dot{x}_{2lo} + f_{2h}^*$ with $\mathcal{Z}_{2h} = m_{2h}s + d_{2h} + k_{2h}/s$. Then, using (25), (33), (48), and (49), we can derive the requirement for the stability of the second local robot and the mobile platform as

$$\begin{aligned}&\left[(C\Lambda_2 + C\Upsilon_2\breve{k}) - (1 + C\Upsilon_2\breve{m})\omega^2\right]^2 +\\ &\left[(C + \Lambda_2 + C\Upsilon_2\breve{d} + C\epsilon_2)\omega\right]^2 - \left[(C - C\Upsilon_2\breve{d})\omega\right]^2 -\\ &\left[(C\Lambda_2 - C\Upsilon_2\breve{k}) + C\Upsilon_2\breve{m}\omega^2\right]^2 \geqslant 0,\end{aligned} \tag{77}$$

where for the mobile platform side, $\breve{m} = 0$, $\breve{d} = 0$, $\breve{k} = 0$, since no contact occurs. For the second local robot side, $\breve{m} = (k_{f2}/k_{p2})m_{2h}$, $\breve{d} = (k_{f2}/k_{p2})d_{2h}$, $\breve{k} = (k_{f2}/k_{p2})k_{2h}$. It is worth mentioning that, if (70) and (71) are not equal to one at the same time, (69) is still guaranteed. Then, to satisfy (77),

$$a_2\omega^4 + b_2\omega^2 + c_2 \geqslant 0 \tag{78}$$

should hold.

Since $a_2 > 0$ and $c_2 \geqslant 0$, the condition for (78) is

$$b_2 + 4C\sqrt{\Lambda_2\Upsilon_2\breve{k}(1 + 2C\Upsilon_2\breve{m})} \geqslant 0. \tag{79}$$

In summary, the proposed dual-user teleoperation approach is stable against arbitrary time delays as long as (75), (76), (78), and (79) are satisfied.

VI. Experimental Setup and Results

To verify the efficiency of the proposed approach, several experiments have been conducted. The experimental setup is introduced in Section VI-A. Section VI-B presents the preliminary results of the task-priority-based redundancy resolution approach with joint-level adaptive controller for a WMM. Section VI-C verifies the proposed dual-user teleoperation approach's performance by achieving a door-opening task in a constrained environment with an obstacle on the ground.

A. Experimental Setup

A three-DOF Phantom Premium 1.5A robot (Geomagic Inc., Wilmington, MA, USA) with a 50M31 F/T sensor (JR3 Inc., Woodland, CA, USA) is employed as the first local robot, a two-DOF Quanser robot (Quanser Consulting Inc., Markham, ON, Canada) with an Axia80-ZC22 F/T sensor (ATI Industrial Automation, Apex, NC, USA) as the second local robot, and an omnidirectional WMM with an Axia80-ZC22 F/T sensor (ATI Industrial Automation, Apex, NC, USA) as the remote robot. The WMM comprises a custom-built four-wheel mobile platform with two pairs of Mecanum wheels and a seven-DOF serial robotic Gen3 arm (Kinova Robotics, Canada). The control system is implemented at a frequency of 1000 Hz (1 ms per loop). It should be emphasized that the MP in the experiments can only be driven via joint velocity rather than joint torque. Thus, an admittance interface is adopted [35].

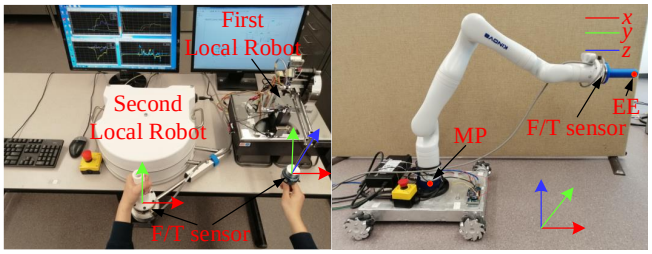

Fig. 2: Experimental setup.

The first local system controls the WMM's EE position, and the second local system dominates the MP's translational motion; thus, $n_1 = 3$, $n_2 = 2$. The initial generalized coordinate vector of the WMM is $q_{re0} = [0, 0, 0, 0, \pi/6, 0, \pi/2, 0, -\pi/6, 0]^{\mathrm{T}}$, where the first three parameters are for the MP. The start positions of the EE and the MP can then be derived using the WMM forward kinematics as $x_{ee0} = [0.8435, -0.0246, 0.4921]^{\mathrm{T}}$ m and $x_{mp0} = [0, 0]^{\mathrm{T}}$ m.

A video is attached with the manuscript to present the experiments in this section.

B. Experiments for Task-Priority-Based Redundancy Resolution of WMM

The admittance interface for each joint of the wheels is defined as $\tau_{mp} = M_{mp}\dot{v}_{mp} + D_{mp}v_{mp}$, where $\tau_{mp} \in \mathbb{R}^{\bar{n}_{mp}}$ denotes the resultant joint torque vector for the MP via (15), $M_{mp} \in \mathbb{R}^{\bar{n}_{mp}\times\bar{n}_{mp}}$ and $D_{mp} \in \mathbb{R}^{\bar{n}_{mp}\times\bar{n}_{mp}}$ are diagonal positive-definite matrices representing the virtual inertia and damping of the interface, respectively. In the experiments, these matrices are selected as $M_{mp} = 0.75I_{4\times4}$ Nm·s^2 and $D_{mp} = 2.4I_{4\times4}$ Nm·s. The controller utilized in the experiments is shown in (15) and (30), and the control parameters are enumerated in Table I of the supplementary material. Three scenarios with different trajectories for the EE and the MP are considered. The first scenario is both two trajectories can be tracked. The second scenario keeps the MP immobile while defining a trajectory for the EE. The third scenario keeps the EE motionless but providing a trajectory for the MP.

The desired trajectories for the EE and the MP are defined as $x^d_{ee}(t) = x_{ee0} + [R_{ee}\sin(\pi/10t), -R_{ee}/2\sin(\pi/5t), 0]^{\mathrm{T}}$ and $x^d_{mp}(t) = x_{mp0} + [-R_{mp}\cos(\pi/10t) + R_{mp}, -R_{mp}\sin(\pi/10t)]^{\mathrm{T}}$, respectively. The required velocities are then defined as $\dot{x}^r_{ee}(t) = \dot{x}^d_{ee}(t) + \Gamma_e[x^d_{ee}(t) - x_{ee}(t)]$ and $\dot{x}^r_{mp}(t) = \dot{x}^d_{mp}(t) + \Gamma_p[x^d_{mp}(t) - x_{mp}(t)]$ to ensure the trajectory tracking error converges to zero, where Γ_e and Γ_p are two diagonal positive-definite matrices with $\Gamma_e = 3.2I_{3\times3}$ and $\Gamma_p = 1.6I_{2\times2}$. The proof of trajectory convergence can be found in Section V-D of the supplementary material. The values of the two gains are obtained by trial and error in this research; furthermore, an approach to optimize their values can be found in [36]. The trajectory parameters in the three scenarios are as follows. **Scenario 1:** $R_{ee} = 0.2$ m, $R_{mp} = 0.2$ m; **Scenario 2:** $R_{ee} = 0.25$ m, $R_{mp} = 0$ m; **Scenario 3:** $R_{ee} = 0$ m, $R_{mp} = -0.15$ m.

The experimental results are presented in Figs. 3-7 for the three scenarios. It is worth mentioning that, first, the desired trajectory for the EE is defined in the $x - y$ plane; thus, the tracking results in the z direction are not provided. Second, the EE's initial position is subtracted from its trajectory to better present the EE and MP trajectories in one figure.

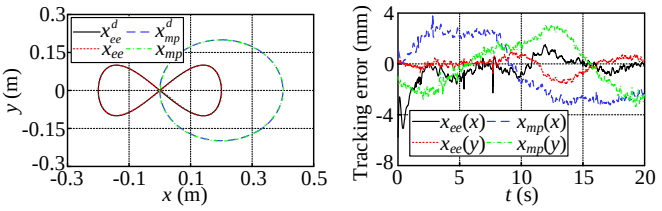

(a) Trajectories (b) Tracking errors

Fig. 3: Trajectory tracking results in **Scenario 1**.

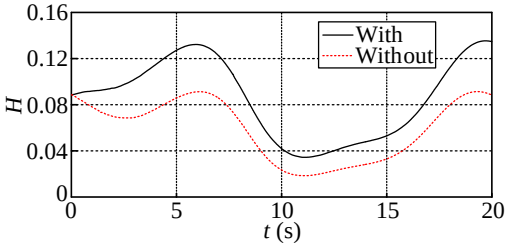

Fig. 4: Profile of cost function for singularity avoidance in **Scenario 1**.

Fig. 3 shows that when the WMM had enough redundancy to realize the control required for the EE and MP simultaneously, both of their trajectories could be tracked. The

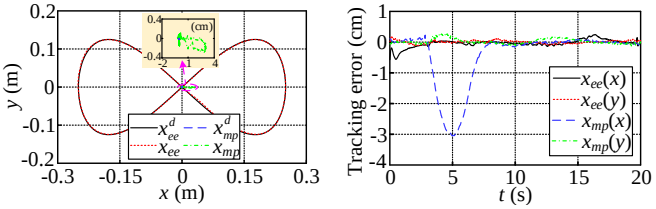

(a) Trajectories (b) Tracking errors

Fig. 5: Trajectory tracking results in **Scenario 2**.

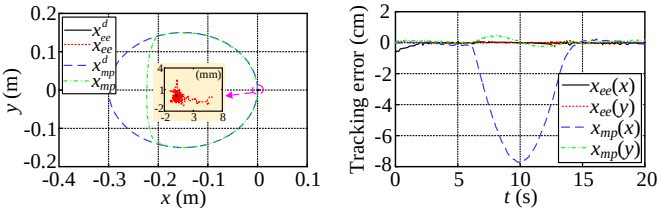

(a) Trajectories (b) Tracking errors

Fig. 6: Trajectory tracking results in **Scenario 3**.

maximum tracking error occurred at y direction of the EE trajectory, which was about 5 mm, representing 1.25% of its commanded motion range. Fig. 4 presents the singularity measure profile defined in (35) during **Scenario 1**. With the singularity avoidance approach executed as the tertiary task, the average value of H was augmented from 0.0587 to 0.0855, approximately a half bigger than its previous value.

In **Scenario 2**, the redundancy of the WMM was deficient in tracking the EE trajectory while keeping the MP immobile. With the higher tracking priority of the EE trajectory, the MP was forced to move to follow the EE's desired trajectory (shown in Fig. 5). As shown in Fig. 5b, the MP was compelled to move about 3 cm during 2.85-8.09 s in x direction, and the maximum tracking error of the EE was not more than 6 mm.

Fig. 6 presents the experimental results in the case that the MP should track a given trajectory, which was beyond the WMM's capability if the EE ought to be immovable (**Scenario 3**). With the proposed approach, the MP sacrificed its tracking precision to realize the EE's immobility, as shown in Fig. 6a. From Fig. 6b, the maximum tracking error of the MP in x direction reached approximately 8 cm, while the motion of the EE was less than 6 mm.

Fig. 7 presents the singularity measure in both the last two scenarios. When the two tasks conflicted with each other (2.85-8.09 s for **Scenario 2** and 6.2-13.4 s for **Scenario 3**), the damped least-squares pseudoinverse approach in (36) and (37) for $J_{2re}N_{1re}$ took effect. The singularity measure could be maintained at about 0.008 with no strong vibration during the transition phrases by adopting this method.

C. Experiment for Dual-User Teleoperation of WMM

The teleoperation experiment was executed by a single person via two hands. As shown in Fig. 2, the left hand (second local user) operated the second local robot to control the MP, and the right hand (first local user) manipulated the first local robot to govern the EE. The control parameters in

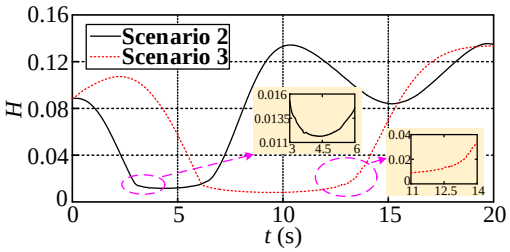

Fig. 7: Profiles of cost function for singularity avoidance in **Scenarios 2 and 3**.

the experiment are provided in the supplementary material. In these control parameters, the method on how to select $\mathcal{K}_{1lo}$, $\mathcal{K}_{2lo}$, $\mathcal{K}_{re}$, Λ_1, and Λ_2 is the same as the determination of Γ_e and Γ_p. Line search techniques [37] are preferable to determine the value of the step size η. The values of singularity avoidance thresholds k_0 and $\sigma_{ma,\min}$ are determined by trial and error to make the system put off the activation time of the damped pseudoinverse as much as possible.

In this section, opening a door with an obstacle on the ground was selected as the task. Some pictures during the experiment are provided in the supplementary material, indicating the success of the door-opening task in a constrained environment via dual-user teleoperation. At first, the left hand manipulated the second local robot to drive the MP to avoid the obstacle. After the obstacle was bypassed, the right hand operated the first local robot to move the EE to open the door, while the left hand employed the second local robot to move the MP to follow the EE. Finally, the WMM successfully opened the door through the user's teleoperation, with the obstacle avoided. Here, the door in the experiment is a fireproof door with heavy resistance torque. Virtual joint torque limits are set for all manipulator's joints to keep the safety of the experimentation. When one of the limits is reached, the test will be stopped automatically.

We have conducted three groups of experiments to prove the effectiveness of the proposed dual-user teleoperation approach. Table III in the supplementary material presents the door-opening results for each experiment, including the position/force tracking errors and the execution time. Also, we introduce two normalizing performance indicators $\chi_p = \max\left(\frac{\|k_p x_{lo} - x_{re}\|_2}{\|\dot{x}_{re}\|_2}\right)$ and $\chi_f = \max\left(\frac{\|k_{f1} f_{1h} - f_{ee}\|_2}{\|\dot{x}_{ee}\|_2}\right)$ to evaluate the motion and force tracking performance, respectively. Here, in χ_p, $k_p \in \{k_{p1}, k_{p2}\}$, $x_{lo} \in \{x_{1lo}, x_{2lo}\}$, $x_{re} \in \{x_{ee}, x_{mp}\}$. A similar motion performance indicator χ_p was adopted in [34].

From the table, we can see that the maximum position tracking error was no more than 3.12 mm during the three experiments. The RMS value of the force tracking errors was less than 0.47 N. The average time of the door-opening task was approximately 78.7 s. Besides, the position and force performance indicators were below 0.097 s and 91.68 N·s/m, respectively. These results demonstrate both the validity and reliability of the proposed method.

Furthermore, Figs. 8-10 provide the results of the first teleoperation experiment in detail, where Figs. 8 and 10a show

the position and force tracking profiles of the primary task, and Figs. 9 and 10b present the position tracking and human force profiles of the secondary task.

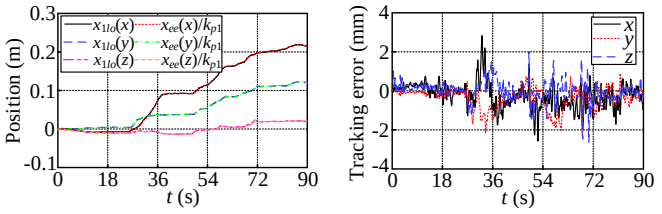

(a) Trajectories (b) Tracking errors

Fig. 8: Trajectory tracking results of the primary task.

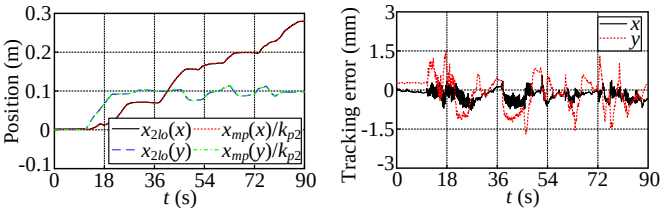

(a) Trajectories (b) Tracking errors

Fig. 9: Trajectory tracking results of the secondary task.

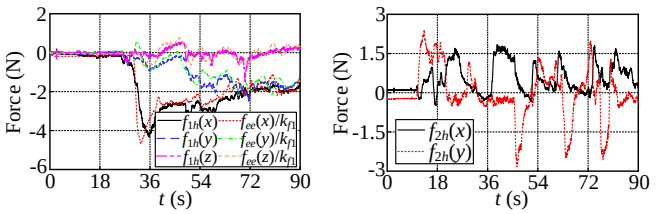

(a) End-effector force tracking (b) Second local user force

Fig. 10: Measured forces during the teleoperation experiment.

Fig. 9a shows that the MP was motivated in y direction at 10.84 s to avoid the obstacle. After that, the MP was activated in x direction from 20.40 s to move it forward. Fig. 9b shows that the maximum tracking error between the second local robot position and the scaled MP position was only approximately 1.69 mm. Fig. 10b presents that the second local user could exert a small force (no more than 3 N) to control the MP, which was proved in (53).

Figs. 8a and 10a display that the motion of the EE was started at about 26.50 s; and the door started to be opened from 29.22 s, which was performed after the MP circumvented the obstacle. To open the door, as shown in Fig. 8a, the final displacements of the WMM's EE were about 0.657 m, 0.369 m, and 0.062 m in x, y, and z, respectively. The maximum position tracking error was 2.83 mm, exhibited in Fig. 8b. Fig. 10a shows that the door's maximum resistant force was about 27.9 N, occurred at about 32.88 s in x direction. As the door opened, the x force decreased while the y force increased. For the tracking results between the first local robot force and the scaled EE force, they could track each other after a steady contact was established (40.5-90 s), with the maximum tracking error being 1.02 N. This is the experimental verification of the theoretical conclusion in (47).

D. Experiment Under Time Delay

Constant delays $T_1 = 50\,\text{ms}$ and $T_2 = 70\,\text{ms}$ for both the motion and force transmission are implemented to verify the proposed method against time delay, which is theoretically proved in Section V-B. The other control parameters are set the same as in Section VI-C. Figs. 11-12 present the experimental results of the position-force teleoperation, which are comparable with the no time delay teleoperation results, as shown in Figs. 8-10, proving the method's capability in handling time delay without severe loss of tracking performance.

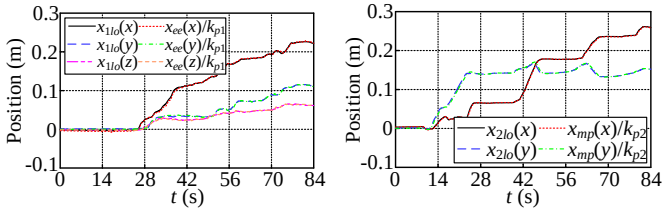

(a) Primary task (b) Secondary task

Fig. 11: Position tracking results under time delay.

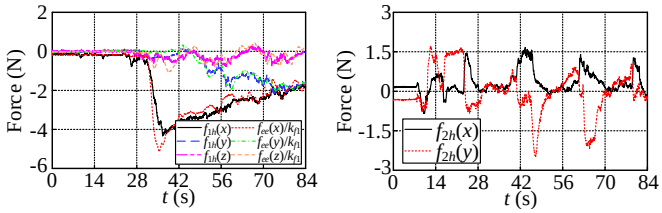

(a) End-effector force tracking (b) Second local user force

Fig. 12: Measured forces of the teleoperation under time delay.

VII. Conclusions

This paper proposes a dual-user teleoperation approach for a redundant wheeled mobile manipulator (WMM), which realizes the separate control of the end-effector (EE) and the mobile platform (MP) via a task-priority framework. The first local robot controls the EE, and the second local robot manipulates the MP. The separate control of the EE and the MP using two local robots is realized by a task-priority-based redundancy resolution method. Any remaining redundancy of the WMM is utilized to enhance the WMM's capability to keep it from the singularity.

The experimental verification in this paper is divided into two sections. The first section proves the effectiveness of the task-priority-based redundancy resolution approach, with the maximum position tracking error no more than 6 mm. The second is the demonstration of the dual-user teleoperation framework, where a door-opening task in a restrained environment with an obstacle on the ground is selected. Three groups of experiments were conducted. The first local robot position/scaled EE position and the second local robot

position/scaled MP position could track each other respectively, with the maximum tracking error less than 1.29% of its motion range. The force tracking result shows that the first local user could feel the scaled contact force exerted at the EE with the largest force error of about 1 N when the contact turned stable. The force exerted by the second local user kept small (less than 3 N) to control the MP, as proved by the theoretical analysis. The performance of the teleoperation approach against arbitrary time delays has also been experimentally verified.

In future work, we will consider making an autonomous controller control the MP motion to reduce the operator's operation pressure. Other aspects worth exploring are merging the superiority of learning from demonstration technique and teleoperation to make the controller more intelligent.

REFERENCES

[1] H. Xing, K. Xia, L. Ding, H. Gao, G. Liu, and Z. Deng, "Unknown geometrical constraints estimation and trajectory planning for robotic door-opening task with visual teleoperation assists," *Assembly Automation*, vol. 39, no. 3, pp. 479–488, 2019.

[2] J. Li, B. You, L. Ding, X. Yu, W. Li, T. Zhang, and H. Gao, "Dual-master/single-slave haptic teleoperation system for semiautonomous bilateral control of hexapod robot subject to deformable rough terrain," *IEEE Transactions on Systems, Man, and Cybernetics: Systems*, pp. 1–15, 2021.

[3] W. Li, L. Ding, H. Gao, and M. Tavakoli, "Haptic tele-driving of wheeled mobile robots under nonideal wheel rolling, kinematic control and communication time delay," *IEEE Transactions on Systems, Man, and Cybernetics: Systems*, vol. 50, no. 1, pp. 336–347, 2020.

[4] M. Shahbazi, S. F. Atashzar, H. A. Talebi, and R. V. Patel, "An expertise-oriented training framework for robotics-assisted surgery," in *IEEE International Conference on Robotics and Automation*, 2014, pp. 5902–5907.

[5] A. Mörtl, M. Lawitzky, A. Kucukyilmaz, M. Sezgin, C. Basdogan, and S. Hirche, "The role of roles: Physical cooperation between humans and robots," *The International Journal of Robotics Research*, vol. 31, no. 13, pp. 1656–1674, 2012.

[6] H. Xing, A. Torabi, L. Ding, H. Gao, Z. Deng, and M. Tavakoli, "Enhancement of force exertion capability of a mobile manipulator by kinematic reconfiguration," *IEEE Robotics and Automation Letters*, vol. 5, no. 4, pp. 5842–5849, 2020.

[7] J. Park and O. Khatib, "A haptic teleoperation approach based on contact force control," *The International Journal of Robotics Research*, vol. 25, no. 5-6, pp. 575–591, 2006.

[8] M. A. R. Garcia, R. A. Rojas, and F. Pirri, "Object-centered teleoperation of mobile manipulators with remote center of motion constraint," *IEEE Robotics and Automation Letters*, vol. 4, no. 2, pp. 1745–1752, 2019.

[9] A. Pepe, D. Chiaravalli, and C. Melchiorri, "A hybrid teleoperation control scheme for a single-arm mobile manipulator with omnidirectional wheels," in *IEEE/RSJ International Conference on Intelligent Robots and Systems*, 2016, pp. 1450–1455.

[10] D. Santiago, E. Slawinski, and V. Mut, "Human-inspired stable bilateral teleoperation of mobile manipulators," *ISA Transactions*, vol. 95, pp. 392–404, 2019.

[11] S. Sirouspour, "Modeling and control of cooperative teleoperation systems," *IEEE Transactions on Robotics*, vol. 21, no. 6, pp. 1220–1225, 2005.

[12] J. Li, M. Tavakoli, and Q. Huang, "Stability of cooperative teleoperation using haptic devices with complementary degrees of freedom," *IET Control Theory & Applications*, vol. 8, no. 12, pp. 1062–1070, 2014.

[13] M. Agbalé, R. Ocampo, and M. Tavakoli, "User's task performance in two-handed complementary-motion teleoperation," in *IEEE International Conference on Robotics and Automation*, 2016, pp. 2682–2687.

[14] P. Malysz and S. Sirouspour, "A kinematic control framework for single-slave asymmetric teleoperation systems," *IEEE Transactions on Robotics*, vol. 27, no. 5, pp. 901–917, 2011.

[15] P. Malysz and S. Sirouspour, "Trilateral teleoperation control of kinematically redundant robotic manipulators," *The International Journal of Robotics Research*, vol. 30, no. 13, pp. 1643–1664, 2011.

[16] F. Farelo, R. Alqasemi, and R. Dubey, "Optimized dual-trajectory tracking control of a 9-dof wmra system for adl tasks," in *IEEE International Conference on Robotics and Automation*, 2010, pp. 1786–1791.

[17] B. Siciliano, "Kinematic control of redundant robot manipulators: A tutorial," *Journal of Intelligent and Robotic Systems*, vol. 3, no. 3, pp. 201–212, 1990.

[18] M. Mashali, R. Alqasemi, and R. Dubey, "Task priority based dual-trajectory control for redundant mobile manipulators," in *IEEE International Conference on Robotics and Biomimetics*, 2014, pp. 1457–1462.

[19] M. Shahbazi, S. F. Atashzar, M. Tavakoli, and R. V. Patel, "Position-force domain passivity of the human arm in telerobotic systems," *IEEE/ASME Transactions on Mechatronics*, vol. 23, no. 2, pp. 552–562, 2018.

[20] W.-H. Zhu and S. E. Salcudean, "Stability guaranteed teleoperation: an adaptive motion/force control approach," *IEEE Transactions on Automatic Control*, vol. 45, no. 11, pp. 1951–1969, 2000.

[21] A. Torabi, M. Khadem, K. Zareinia, G. R. Sutherland, and M. Tavakoli, "Using a redundant user interface in teleoperated surgical systems for task performance enhancement," *Robotica*, pp. 1–15, 2020.

[22] R. Kelly, V. S. Davila, and J. A. L. Perez, *Control of robot manipulators in joint space*. Springer Science & Business Media, 2006.

[23] C. Yang, G. Peng, L. Cheng, J. Na, and Z. Li, "Force sensorless admittance control for teleoperation of uncertain robot manipulator using neural networks," *IEEE Transactions on Systems, Man, and Cybernetics: Systems*, pp. 1–11, 2019.

[24] G. D. White, R. M. Bhatt, C. P. Tang, and V. N. Krovi, "Experimental evaluation of dynamic redundancy resolution in a nonholonomic wheeled mobile manipulator," *IEEE/ASME Transactions on Mechatronics*, vol. 14, no. 3, pp. 349–357, 2009.

[25] M. Iskandar, G. Quere, A. Hagengruber, A. Dietrich, and J. Vogel, "Employing whole-body control in assistive robotics," in *IEEE International Conference on Intelligent Robots and Systems*, 2019, pp. 5643–5650.

[26] A. De Luca, G. Oriolo, and P. R. Giordano, "Kinematic modeling and redundancy resolution for nonholonomic mobile manipulators," in *IEEE International Conference on Robotics and Automation*, 2006, pp. 1867–1873.

[27] H. Lu, L. Jin, J. Zhang, Z. Sun, S. Li, and Z. Zhang, "New joint-drift-free scheme aided with projected znn for motion generation of redundant robot manipulators perturbed by disturbances," *IEEE Transactions on Systems, Man, and Cybernetics: Systems*, pp. 1–13, 2019.

[28] Y. Nakamura, H. Hanafusa, and T. Yoshikawa, "Task-priority based redundancy control of robot manipulators," *The International Journal of Robotics Research*, vol. 6, no. 2, pp. 3–15, 1987.

[29] F. Flacco, A. De Luca, and O. Khatib, "Control of redundant robots under hard joint constraints: Saturation in the null space," *IEEE Transactions on Robotics*, vol. 31, no. 3, pp. 637–654, 2015.

[30] A. Escande, N. Mansard, and P.-B. Wieber, "Hierarchical quadratic programming: Fast online humanoid-robot motion generation," *The International Journal of Robotics Research*, vol. 33, no. 7, pp. 1006–1028, 2014.

[31] H. Zhang, Y. Jia, and N. Xi, "Sensor-based redundancy resolution for a nonholonomic mobile manipulator," in *IEEE/RSJ International Conference on Intelligent Robots and Systems*, 2012, pp. 5327–5332.

[32] T. Yoshikawa, "Manipulability of robotic mechanisms," *The International Journal of Robotics Research*, vol. 4, no. 2, pp. 3–9, 1985.

[33] R. V. Patel and F. Shadpey, *Control of redundant robot manipulators: theory and experiments*. Springer Science & Business Media, 2005.

[34] S. Lampinen, J. Koivumäki, W.-H. Zhu, and J. Mattila, "Force-sensorless bilateral teleoperation control of dissimilar master-slave system with arbitrary scaling," *IEEE Transactions on Control Systems Technology*, pp. 1–15, 2021.

[35] A. Dietrich, K. Bussmann, F. Petit, P. Kotyczka, C. Ott, B. Lohmann, and A. Albu-Schäffer, "Whole-body impedance control of wheeled mobile manipulators," *Autonomous Robots*, vol. 40, no. 3, pp. 505–517, 2016.

[36] J.-J. Slotine and L. Weiping, "Adaptive manipulator control: A case study," *IEEE Transactions on Automatic Control*, vol. 33, no. 11, pp. 995–1003, 1988.

[37] D. G. Luenberger and Y. Ye, *Linear and Nonlinear Programming*. Springer, 1984.

Dual-User Haptic Teleoperation of Complementary Motions of a Redundant Wheeled Mobile Manipulator Considering Task Priority -Supplementary material-

Hongjun Xing, Liang Ding, Haibo Gao, Weihua Li, and Mahdi Tavakoli

***Abstract*—We report some supplementary materials in this document to the manuscript.**

I. A Motivating Example

We provide a dual-user haptic teleoperation approach for a WMM to conduct complex tasks in a constrained environment via two local robots, such as rescue tasks. The first local robot controls the position of the EE. In contrast, the second local robot manipulates that of the MP in the null space of the robotic system to avoid intervening in the main task. The dual-user teleoperation is adopted because if only the EE position is controlled, the tasks in a constrained environment sometimes cannot be completed [1]. Here, a door-opening operation performed by a human in an environment with overground obstacles is used to demonstrate the concept of the proposed method and the necessity of employing two local robots.

Fig. 1 presents a general diagram of how a human opens a door in a constrained environment. Fig. 1a shows that the human reaches his upper limb to the door's handle. Fig. 1b presents that the human moves his lower limb sideways to avoid the obstacle on the ground. After the human's lower limb circumventing the obstacle, his upper limb will continue to reach and open the door, as exhibited in Fig. 1c. Finally, the human succeeds in opening the door by employing both his limbs, as shown in Fig. 1d. It is noteworthy that for different people, the motion phases in Figs. 1b and 1c may be integrated. Nonetheless, the person still needs to control his upper and lower limbs to achieve different tasks (upper limb for opening the door and lower limb for avoiding the obstacle). Obviously, two local robots are required for tele-manipulating this operation since the controls of the upper limb and the lower limb are independent. If we only control the upper limb's motion, then the path of the lower limb will be inevitably impeded by the obstacle. However, to the best of the authors' knowledge, no research has been done on providing a practical cooperative teleoperation framework for a WMM to deal with assignments in a non-free space; we propose a novel WMM teleoperation method for such tasks.

H. Xing, L. Ding, H. Gao, and W. Li are with the State Key Laboratory of Robotics and System, Harbin Institute of Technology, Harbin 150001, China. (e-mails: {xinghj, liangding, gaohaibo, liweihua}@hit.edu.cn).

W. Li is with the School of Automotive Engineering, Harbin Institute of Technology (Weihai), Weihai 264209, China.

H. Xing and M. Tavakoli are with the Department of Electrical and Computer Engineering, University of Alberta, Edmonton T6G 1H9, Alberta, Canada. (e-mail: mahdi.tavakoli@ualberta.ca).

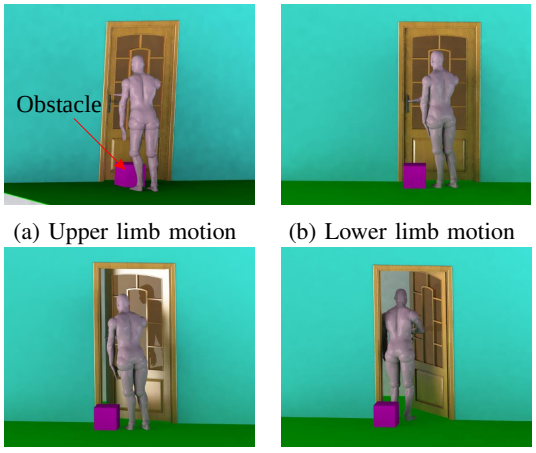

(a) Upper limb motion (b) Lower limb motion

(c) Upper limb motion (d) Both limbs motion

Fig. 1: Illustration of human opening a door in a constrained environment.

II. Detailed Equation Explanation of Section V

Detailed information of eqs. (65) and (66).

$$
\begin{aligned}
\underline{\rho}_{1lo} &\overset{def}{=} \overline{\rho}_{1lo} - \Upsilon_1 k_{f1} k_{p1}^{-1} \tilde{f}_{1h}^{*},\\
\underline{\rho}_{1re} &\overset{def}{=} \overline{\rho}_{1re} - e^{-sT_1} \Upsilon_1 k_{f1} \tilde{f}_{1h}^{*},\\
\mathcal{G}_{1lo1}(s) &\overset{def}{=} (s+\Lambda_1)(C^{-1}s+I) + \Upsilon_1 k_{f1} k_{p1}^{-1} \mathcal{Z}_{1h} s + \epsilon_1 s,\\
\mathcal{G}_{1lo2}(s) &\overset{def}{=} (s+\Lambda_1) I - \Upsilon_1 \mathcal{Z}_e s,\\
\mathcal{G}_{1re1}(s) &\overset{def}{=} (s+\Lambda_1)(C^{-1}s+I) + \Upsilon_1 \mathcal{Z}_e s + \epsilon_1 s,\\
\mathcal{G}_{1re2}(s) &\overset{def}{=} (s+\Lambda_1) I - \Upsilon_1 k_{f1} k_{p1}^{-1} \mathcal{Z}_{1h} s.
\end{aligned}
$$

Detailed information of eqs. (67) and (68).

$$
\begin{aligned}
\rho_{1lo}^{*} &= \mathcal{G}_{1lo1}^{-1}(s) k_{p1} \underline{\rho}_{1lo} + \mathcal{G}_{1lo1}^{-1}(s) \mathcal{G}_{1lo2}(s) \mathcal{G}_{1re1}^{-1}(s) e^{-sT_2} \underline{\rho}_{1re},\\
\rho_{1re}^{*} &= \mathcal{G}_{1re1}^{-1}(s) \underline{\rho}_{1re} + \mathcal{G}_{1re1}^{-1}(s) \mathcal{G}_{1re2}(s) \mathcal{G}_{1lo1}^{-1}(s) e^{-sT_1} k_{p1} \underline{\rho}_{1lo}.
\end{aligned}
$$

Detailed information of eq. (75).

$$
\begin{aligned}
a_1 &= 1 + 2C\Upsilon_1 \breve{m},\\
b_1 &= \Lambda_1^2 + 2C\Upsilon_1(\Lambda_1 \breve{d} - 2C\Lambda_1 \breve{m} +\\
&\quad \epsilon_1 + 2C\breve{d} - \breve{k} + C\epsilon_1 \breve{d}) + C^2(2+\epsilon_1)\epsilon_1,\\
c_1 &= 4C^2 \Lambda_1 \Upsilon_1 \breve{k}.
\end{aligned}
$$

Detailed information of eq. (78).

$$
\begin{aligned}
a_2 &= 1 + 2C\Upsilon_2\breve{m}, \\
b_2 &= \Lambda_2^2 + 2C\Upsilon_2(\Lambda_2\breve{d} - 2C\Lambda_2\breve{m} + \\
&\quad \epsilon_2 + 2C\breve{d} - \breve{k} + C\epsilon_2\breve{d}) + C^2(2+\epsilon_2)\epsilon_2, \\
c_2 &= 4C^2\Lambda_2\Upsilon_2\breve{k}.
\end{aligned}
$$

III. Some Tables of Section VI

The control parameters of the task-priority-based redundancy resolution experiment is listed in Table I.

TABLE I: Control parameters utilized in redundancy resolution experiments.

Parameter	Value
$\mathcal{K}_{re}$(Nm·s)	diag$(5I_{4\times4}, 3I_{7\times7})$
ϱ_{re}	1.5
η	10
k_0	0.1
$\sigma_{ma,\min}$	0.1

The control parameters of the dual-user teleoperation experiment are listed in Table II with some of them already being provided in Table I, where for the diagonal matrices with identical elements, only the scalar gains are provided in the table.

TABLE II: Control parameters adopted in dual-user teleoperation experiment.

Parameter	Value	Parameter	Value
$\mathcal{K}_{1lo}$(Nm·s)	diag$(12, 12, 8)$	$\mathcal{K}_{2lo}$(Nm·s)	8
ϱ_{1lo}	2	ϱ_{2lo}	2
Υ_1(kg^{-1}s)	0.01	Υ_2(kg^{-1}s)	0.01
Λ_1(s^{-1})	4.8	Λ_2(s^{-1})	3.2
ϵ_1	-1.2	ϵ_2	-1.3
k_{p1}	3	k_{p2}	3
k_{f1}	6	k_{f2}	1
C	50		

Table III presents the door-opening results for each experiment, including the position/force tracking errors and the execution time.

IV. Pictures of Section VI.C

Fig. 2 presents some pictures during the dual-user teleoperation experiment, indicating the success of the door-opening task in a constrained environment via dual-user teleoperation.

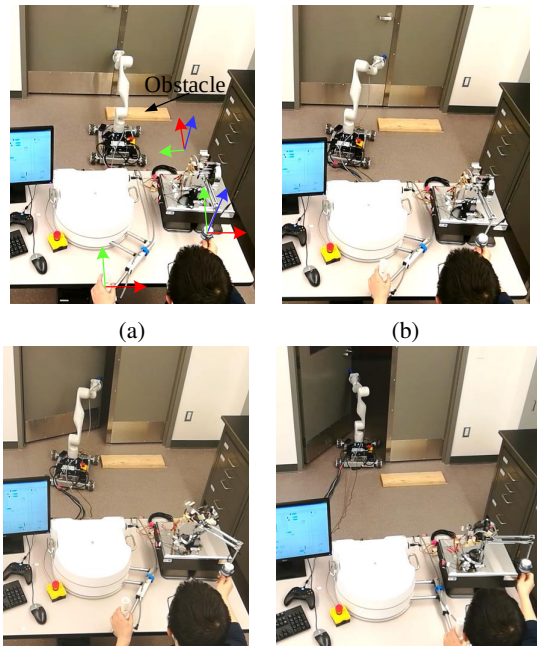

Fig. 2: Pictures of the door-opening experiment via dual-user teleoperation. (a) shows the initial state of the test platform, (b) shows the MP's motion to avoid the obstacle, (c) shows the hybrid movements of the EE and the MP to unlock the door, and (d) shows the final state of the platform with an opened door.

V. Definitions, Lemmas, and Properties

A. Parameter Adaptation

The following projection function in [2] is utilized for parameter adaptation.

Definition 1: A projection function $\mathcal{P}(s(t), k, a(t), b(t), t) \in \mathbb{R}$ is a differentiable scalar function defined in $t \geqslant 0$ such that its time derivative is governed by

$$\dot{\mathcal{P}} = ks(t)\kappa \tag{1}$$

with

$$\kappa = \begin{cases} 0, & \text{if } \mathcal{P} \leqslant a(t) \text{ and } s(t) \leqslant 0 \\ 0, & \text{if } \mathcal{P} \geqslant b(t) \text{ and } s(t) \geqslant 0 \\ 1, & \text{otherwise} \end{cases}$$

where $s(t) \in \mathbb{R}$ is a scalar variable, k is a positive constant and $a(t) \leqslant b(t)$ holds.

Consider an arbitrary $\mathcal{P}$ function defined in (1), and for any constant $\mathcal{P}_c$ satisfying $a(t) \leqslant \mathcal{P}_c \leqslant b(t)$, it follows that

$$(\mathcal{P}_c - \mathcal{P})\left(s(t) - \frac{1}{k}\dot{\mathcal{P}}\right) \leqslant 0. \tag{2}$$

B. Stability Theorem

The following lemmas are used to prove the L_2 and L_∞ stability of the robotic systems.

Lemma 1: Consider a non-negative piecewise continuous function $\xi(t)$ described as

$$\xi(t) \geqslant \frac{1}{2}x(t)^{\mathrm{T}}Px(t), \tag{3}$$

where $x(t) \in \mathbb{R}^n, n \geqslant 1$ and $P \in \mathbb{R}^{n\times n}$ is a symmetric positive-definite matrix. If the derivative of $\xi(t)$ with respect to time is Lebesgue integrable and subject to

$$\dot{\xi}(t) \leqslant -y(t)^{\mathrm{T}}Qy(y) - s(t) \tag{4}$$

with $y(t) \in \mathbb{R}^m, m \geqslant 1$ and $Q \in \mathbb{R}^{m\times m}$ being a symmetric positive-definite matrix, and $s(t)$ is governed by

$$\int_0^\infty s(t)dt \geqslant -\gamma_0 \tag{5}$$

TABLE III: Task-space tracking errors and execution time during teleoperation experiments.

		Position error (mm) Max.	Position error (mm) RMS	Force error (N) Max.	Force error (N) RMS	Execution time (s)	Position index χ_p (s)	Force index χ_f (N·s/m)
Exp. 1	Primary task	2.83	0.68	2.23	0.42	78.1	0.097	91.68
	Secondary task	1.69	0.63	/	/		0.059	/
Exp. 2	Primary task	2.74	0.58	2.15	0.40	83.7	0.082	75.37
	Secondary task	3.12	0.94	/	/		0.091	/
Exp. 3	Primary task	2.88	0.62	2.34	0.47	74.4	0.084	73.43
	Secondary task	1.78	0.69	/	/		0.053	/

with $0 \leqslant \gamma_0 < \infty$, then it follows that $\xi(t) \in L_\infty$, $x(t) \in L_\infty$, and $y(t) \in L_2$ hold.

Lemma 2: Consider a MIMO (multiple-input-multiple-output) first-order system expressed as

$$\dot{x}(t) + Kx(t) = u(t) \tag{6}$$

with $x(t) \in \mathbb{R}^n$, $u(t) \in \mathbb{R}^n$, and $K \in \mathbb{R}^{n\times n}$ being a symmetrical and positive-definite matrix. If $u(t) \in L_2 \cap L_\infty$, then $x(t) \in L_2 \cap L_\infty$ and $\dot{x}(t) \in L_2 \cap L_\infty$.

Lemma 3: Consider a MIMO second-order system illustrated as

$$M\ddot{x}(t) + D\dot{x}(t) + Kx(t) = u(t) \tag{7}$$

with $x(t) \in \mathbb{R}^n$, $u(t) \in \mathbb{R}^n$, and $M \in \mathbb{R}^{n\times n}$, $D \in \mathbb{R}^{n\times n}$, and $K \in \mathbb{R}^{n\times n}$ being symmetrical and positive-definite matrices. If $u(t) \in L_2 \cap L_\infty$, then $x(t) \in L_2 \cap L_\infty$, $\dot{x}(t) \in L_2 \cap L_\infty$, and $\ddot{x}(t) \in L_2 \cap L_\infty$.

Lemma 4: If $e(t) \in L_2$ and $\dot{e}(t) \in L_\infty$, then $\lim_{t\to\infty} e(t) = 0$.

Lemma 4 is of great importance in proving the asymptotic convergence for an error signal $e(t)$.

C. Properties for Pseudoinverse and Null-space Matrices

For the pseudoinverse and null-space matrices in this paper, the following properties are preserved

$$J_{1re}N_{1re} = 0, \quad J_{1re}J_{1re}^{\dagger} = I, \tag{8}$$

$$J_{2re}N_{1re}N_{2|1re} = J_{2re}N_{1re} - J_{2re}N_{1re} = 0, \tag{9}$$

$$N_{1re}N_{2|1re}N_{1re} = N_{1re}N_{2|1re}, \ N_{2|1re}(J_{2re}N_{1re})^{\dagger} = 0, \tag{10}$$

$$N_{2|1re}N_{2|1re} = N_{2|1re}, \ N_{1re}N_{2|1re}J_{1re}^{\dagger} = 0, \tag{11}$$

D. Trajectory Convergence Proof via Velocity Command

When no contact occurs at the WMM's EE, according to eqs. (32) and (33) of the paper, it derives

$$\dot{x}_{ee}^{r} - \dot{x}_{ee} \in L_2 \cap L_\infty, \tag{12}$$

$$\dot{x}_{mp}^{r} - \dot{x}_{mp} \in L_2 \cap L_\infty. \tag{13}$$

With the required velocity definition $\dot{x}_{ee}^{r} = \dot{x}_{ee}^{d} + \Gamma_e(x_{ee}^{d} - x_{ee})$ and $\dot{x}_{mp}^{r} = \dot{x}_{mp}^{d} + \Gamma_p(x_{mp}^{d} - x_{mp})$, we can further derive

$$(\dot{x}_{ee}^{d} - \dot{x}_{ee}) + \Gamma_e(x_{ee}^{d} - x_{ee}) \in L_2 \cap L_\infty, \tag{14}$$

$$(\dot{x}_{mp}^{d} - \dot{x}_{mp}) + \Gamma_p(x_{mp}^{d} - x_{mp}) \in L_2 \cap L_\infty. \tag{15}$$

In line with Lemma 2 of Section V-B, we know

$$\dot{x}_{ee}^{d} - \dot{x}_{ee} \in L_2 \cap L_\infty, \quad x_{ee}^{d} - x_{ee} \in L_2 \cap L_\infty, \tag{16}$$

$$\dot{x}_{mp}^{d} - \dot{x}_{mp} \in L_2 \cap L_\infty, \quad x_{mp}^{d} - x_{mp} \in L_2 \cap L_\infty, \tag{17}$$

then according to Lemma 4 in Section V-B, it derives $\lim_{t\to\infty}(x_{ee}^{d} - x_{ee}) = 0$ and $\lim_{t\to\infty}(x_{mp}^{d} - x_{mp}) = 0$.

REFERENCES

[1] P. Malysz and S. Sirouspour, "Trilateral teleoperation control of kinematically redundant robotic manipulators," *The International Journal of Robotics Research*, vol. 30, no. 13, pp. 1643–1664, 2011.

[2] W. Zhu, *Virtual Decomposition Control - Toward Hyper Degrees of Freedom Robots*. Springer, 2010.